

## IMPACT PROCESS: AN IMPORTANT GEOLOGICAL PHENOMENON

ROMAN SKÁLA

National Museum, Department of Mineralogy and Petrology, Václavské nám. 68, Praha 1, Czech Republic



Skála, R. (1996): Impact process: An important geological phenomenon. - Acta Mus. Nat. Pragae, Ser. B., Hist. Nat., 52(1996)(1-4): 111-156. Praha. ISSN 0036-5343.

Abstract. The impact process was for a long period of time, even after a wider acceptance among the geological community, considered to be a marginal phenomenon in the Earth sciences. The last decade or two have showed an importance of the process itself and consequent events only too clearly. The present paper is a review describing the history and development of the impact hypothesis, structure and origin of impact craters, influence of huge impacts on the living environment and other aspects of the impact process from the point of view of geology s.l.

■ Impact process, mass extinctions, shock metamorphism, impactites, impact structures, meteorite craters.

Received April 23, 1996

### Introduction

Collisions of individual bodies of a very different size ranging from millimeters to orders of tens kilometers traveling at cosmic velocities played a really important role in the evolution of the early Solar system. They provided the heat necessary for the origin of larger accumulations of solid matter - protoplanets. Even after protoplanets had been formed, the so-called Great Bombardment by relatively dense (compared to the recent state of matter) streams of cosmic material represented by meteorites, comets and asteroids as well helped to initiate tectonic and volcanic processes inside terrestrial planets and some satellites of jovian planets that resemble the Earth by their inner structure. Kinetic energy released during these great impacts was in fact one of the starting points leading to the modern face of the Earth-like bodies of our Solar system. The evidence that the impact process is really ubiquitous in space, observers can see on many craters from several microns to thousands km in diameter on both natural cosmic objects (except those mentioned just above on asteroids, two irregular Martian moons, etc.) and man-made satellites and even some meteorites that have reached the Earth show apparent shock features caused by cosmic collisions including severe brecciation. As stated by Melosh (1989) in preface to his book one meteoricists even suggested that future historians will accord the recognition of impact cratering an equal importance with the development of plate tectonics concept.

A typical result of a collision of two cosmic bodies of very different sizes is an impact crater or craters on the surface of the greater so-called target body and the destruction of a projectile (smaller body). Sometimes these structures are named as meteorite craters, impact structures or astroblemes. Such a collision in the case of bodies whose dimensions do not differ significantly leads most frequently to the complete destruction of both bodies. The targets scientifically observed up to now are located in our Solar system only. There are large data sets concerning morphology obtained

from remote sensing of surfaces of planets, moons or asteroids within the Solar system. Other than morphological data are unfortunately available on the structures on the Earth and Moon only. If we focus our attention to the Earth surface we know here some 140 impact structures with diameter greater than 10 meters (see Table 1) where we can find characteristic features accompanying the impact of the extraterrestrial material (Grieve 1990, 1993 - pers. comm., Theriault 1995 - pers. comm.). However, Grieve (1990) has pointed out, that from this impact record about 20% craters are buried beneath the cover of younger strata and are known only on the basis of geophysical research and drilling works. For more details concerning terrestrial impact record see Table 1.

The impact of one cosmic body onto the surface of another one and consequent penetration of an impactor to deeper parts of a target might be potentially of economic interest as can be seen in the case of some ore deposits on the Earth. The astrobleme near Canadian Sudbury is world renowned due to Ni-Cu-Co-PGE- mineralization. The processes leading to the formation of this deposit were initialized by a major impact before about 1.8 Ga. The other Canadian impact structure with economically significant filling consisting of uranium-bearing sandstones, is the Carswell Lake crater. An exploitation of the U-ore deposit was possible only due to the 2 km uplift of the central area of the impact structure. Bowl-shaped craters Red Wing Creek and Ames in USA are oil deposits (Koeberl et al. 1994, and Masaitis 1992). As noted by Masaitis (1992) other impact structures could be utilized in some cases for aircraft navigation (e.g. New Quebec Crater in Canada or El'gygytgyn in Russia), water storage (Lunar Crater in India) and methane storage (Siljan in Sweden), or could serve as a source of local, easy to process, building material (Ries crater in Germany: the City Hall and the St. George Church in Nördlingen are built of suevite - see Fig. 1; Rochechouart in France, the castle of the same name).

In the Earth's history, there are many stratigraphic boundaries connected to biological extinctions. In these short time periods reflecting severely changed living conditions, many groups of animals and/or plants often disappeared. Based on the detailed stratigraphic, sedimentological, petrologic, geochemical etc. studies, many scientists all over the world join these cataclysmic events with major impacts and/or their more or less immediate consequences.

In the Czech Republic, there are two probable impact structures not included on the list in the



**Fig. 1. St. John's Church (a) and City Hall (b) in Nördlingen, Germany, built of suevite - an example of the use of local impactite for building purposes.**

**Table 1. List of terrestrial impact record. Data kindly provided by Dr. Ann Therriault of the Geological Survey of Canada. Age and diameter of the Kara structure, Russia, according to Nazarov et al. (1993). Diameter of the Chicxulub crater taken from Sharpton et al. (1993). Age of the Manson structure according to Deutsch and Schärer (1994).**

No.	Crater name	Location	Diameter in km	Age in Ma	Latitude	Longitude
1	Acraman	South Australia, Australia	90	>450	S 32° 1'	E 135° 27'
2	Ames	Oklahoma, USA	16	470	N 36° 15'	W 98° 12'
3	Amguid	Algeria	0.45	<0.1	N 26° 5'	E 4° 23'
4	Aorounga	Chad	12.6	<0.004	N 19° 6'	E 19° 15'
5	Aouelloul	Mauritania	0.39	3.1	N 20° 15'	W 12° 41'
6	Araguainha Dome	Brazil	40	247	S 16° 47'	W 52° 59'
7	Avak	Alaska, USA	12	>95	N 71° 15'	W 156° 38'
8	Azuara	Spain	30	<130	N 41° 10'	W 0° 55'
9	B. P. Structure	Libya	2.8	<120	N 25° 19'	E 24° 20'
10	Barringer	Arizona, USA	1.19	0.05	N 35° 2'	W 111° 1'
11	Beaverhead	Montana, USA	60	600	N 44° 36'	W 113° 0'
12	Beyenchime -Salaatin	Russia	8	<65	N 71° 50'	E 123° 30'
13	Bigach	Kazakhstan	7	6	N 48° 30'	E 82° 0'
14	Boltysch	Ukraine	24	88	N 48° 45'	E 32° 10'
15	Bosumtwi	Ghana	10.5	1.03	N 6° 30'	W 1° 25'
16	Boxhole	Northern Territory, Australia	0.17	0.03	S 22° 37'	E 135° 12'
17	Brent	Ontario, Canada	3.8	450	N 46° 5'	W 78° 29'
18	Campo del Cielo	Argentina	0.05	<0.004	S 27° 38'	W 61° 42'
19	Carswell	Saskatchewan, Canada	39	115	N 58° 27'	W 109° 30'
20	Charlevoix	Quebec, Canada	54	357	N 47° 32'	W 70° 18'
21	Chesapeake Bay	Virginia, USA	85	35.5	N 37° 15'	W 76° 5'
22	Chicxulub	Yucatan, Mexico	170	64.98	N 21° 20'	W 89° 30'
23	Chiyli	Kazakhstan	5.5	46	N 49° 10'	E 57° 51'
24	Chukcha	Russia	6	<70	N 75° 42'	E 97° 48'
25	Clearwater Lake East	Quebec, Canada	26	290	N 56° 5'	W 74° 7'
26	Clearwater Lake West	Quebec, Canada	36	290	N 56° 13'	W 74° 30'
27	Connolly Basin	Western Australia, Australia	9	<60	S 23° 32'	E 124° 45'
28	Crooked Creek	Missouri, USA	7	320	N 37° 50'	W 91° 23'
29	Dalgaranga	Western Australia, Australia	0.02	0.03	S 27° 43'	E 117° 15'
30	Decaturville	Missouri, USA	6	<300	N 37° 54'	W 92° 43'
31	Deep Bay	Saskatchewan, Canada	13	100	N 56° 24'	W 102° 59'
32	Dellen	Sweden	19	89	N 61° 55'	E 16° 39'
33	Des Plaines	Illinois, USA	8	<280	N 42° 3'	W 87° 52'
34	Dobeles	Latvia	4.5	300	N 56° 35'	E 23° 15'
35	Eagle Butte	Alberta, Canada	10	<65	N 49° 42'	W 110° 30'
36	Engygytgyn	Russia	18	3.5	N 67° 30'	E 172° 0'
37	Flynn Creek	Tennessee, USA	3.55	360	N 36° 17'	W 85° 40'
38	Gardnos	Norway	5	500	N 60° 39'	E 9° 10'
39	Glasford	Illinois, USA	4	<430	N 40° 36'	W 89° 47'
40	Glover Bluff	Wisconsin, USA	8	<500	N 43° 58'	W 89° 32'
41	Goat Paddock	Western Australia, Australia	5.1	<50	S 18° 20'	E 126° 40'
42	Gosses Bluff	Northern Territory, Australia	22	142.5	S 23° 50'	E 132° 19'

No.	Crater name	Location	Diameter in km	Age in Ma	Latitude	Longitude
43	Gow Lake	Saskatchewan, Canada	5	<250	N 56° 27'	W 104° 29'
44	Granby	Sweden	3	470	N 58° 25'	E 15° 56'
45	Gusev	Russia	3.5	65	N 48° 21'	E 40° 14'
46	Gweni-Fada	Chad	14	<345	N 17° 25'	E 21° 45'
47	Houghton	Northwest Territorries, Canada	24	23	N 75° 22'	W 89° 41'
48	Haviland	Kansas, USA	0.02	<0.001	N 37° 35'	W 99° 10'
49	Henbury	Northern Territory, Australia	0.16	<0.005	S 24° 35'	E 133° 9'
50	Holleford	Ontario, Canada	2.35	550	N 44° 28'	W 76° 38'
51	Ile Rouleau	Quebec, Canada	4	<300	N 50° 41'	W 73° 53'
52	Ilumetsa	Estonia	0.08	>0.002	N 57° 58'	E 25° 25'
53	Ilyinets	Ukraine	4.5	395	N 49° 6'	E 29° 12'
54	Iso-Naakkima	Finland	3	>1000	N 62° 11'	E 27° 9'
55	Janisjärvi	Russia	14	698	N 61° 58'	E 30° 55'
56	Kaalijärvi	Estonia	0.11	0	N 58° 24'	E 22° 40'
57	Kalkkop	RSA	0.64	<1.8	S 32° 43'	E 24° 34'
58	Kaluga	Russia	15	380	N 54° 30'	E 36° 15'
59	Kamensk	Russia	25	49	N 48° 20'	E 40° 15'
60	Kara	Russia	120	67.27	N 69° 5'	E 64° 18'
61	Kara-Kul	Tadzhikistan	52	<5	N 39° 1'	E 73° 27'
62	Kardla	Estonia	4	455	N 58° 59'	E 22° 40'
63	Karla	Rusko	12	<10	N 54° 54'	E 48° 0'
64	Kelly West	Northern Territory, Australia	10	>550	S 19° 56'	E 133° 57'
65	Kentland	Indiana, USA	13	<97	N 40° 45'	W 87° 24'
66	Kursk	Russia	5.5	250	N 51° 40'	E 36° 0'
67	Lac Couture	Quebec, Canada	8	430	N 60° 8'	W 75° 20'
68	Lac la Moinerie	Quebec, Canada	8	400	N 57° 26'	W 66° 37'
69	Lappajärvi	Finland	23	77.3	N 63° 12'	E 23° 42'
70	Lawn Hill	Queensland, Australia	18	>515	S 18° 40'	E 138° 39'
71	Liverpool	Northern Territory, Australia	1.6	150	S 12° 24'	E 134° 3'
72	Lockne	Sweden	7	>455	N 63° 0'	E 14° 48'
73	Logancha	Russia	20	25	N 65° 30'	E 95° 50'
74	Logoisk	Belorussia	17	40	N 54° 12'	E 27° 48'
75	Lonar	India	1.83	0.05	N 19° 58'	E 76° 31'
76	Lumparn	Finland	9	1 000	N 60° 12'	E 20° 6'
77	Macha	Russia	0.3	<0.007	N 59° 59'	E 118° 0'
78	Manicouagan	Quebec, Canada	100	214	N 51° 23'	W 68° 42'
79	Manson	Iowa, USA	35	73.8	N 42° 35'	W 94° 33'
80	Marquez Dome	Texas, USA	13	58	N 31° 17'	W 96° 18'
81	Middlesboro	Kentucky, USA	6	<300	N 36° 37'	W 83° 44'
82	Mien	Sweden	9	121	N 56° 25'	E 14° 52'
83	Mishina Gora	Russia	4	<360	N 58° 40'	E 28° 0'
84	Mistastin	Newfoundland/ Labrador, Canada	28	38	N 55° 53'	W 63° 18'
85	Mizarai	Lithuania	5	570	N 54° 1'	E 24° 34'
86	Montagnais	Nova Scotia, Canada	45	50.5	N 42° 53'	W 64° 13'
87	Monturaqui	Chile	0.46	<1	S 23° 56'	W 68° 17'
88	Morasko	Poland	0.1	0.01	N 55° 29'	E 16° 54'
89	New Quebec	Quebec, Canada	3.44	1.4	N 61° 17'	W 73° 40'
90	Newporte	North Dakota, USA	3	<500	N 48° 58'	W 101° 58'
91	Nicholson Lake	Nortwest Territories, Canada	12.5	<400	N 62° 40'	W 102° 41'
92	Oasis	Libya	11.5	<120	N 24° 34'	E 24° 24'
93	Obolon'	Ukraine	15	215	N 49° 30'	E 32° 53'
94	Odessa	Texas, USA	0.17	<0.05	N 31° 45'	W 102° 29'
95	Ouarkziz	Algeria	3.5	<70	N 29° 0'	W 7° 33'
96	Piccaninny	Western Australia, Australia	7	<360	S 17° 32'	E 128° 25'

No.	Crater name	Location	Diameter in km	Age in Ma	Latitude	Longitude
97	Pilot Lake	Nortwest Territories, Canada	6	445	N 60° 17'	W 111° 1'
98	Popigai	Russia	100	35	N 71° 30'	E 111° 0'
99	Presqu'île	Quebec, Canada	24	<500	N 49° 43'	W 74° 48'
100	Pretoria Salt Pan	RSA	1.13	0.22	S 25° 44'	E 28° 5'
101	Puchezh -Katunki	Russia	80	175	N 57° 6'	E 43° 35'
102	Ragozinka	Russia	9	55	N 58° 18'	E 62° 0'
103	Red Wing	North Dakota, USA	9	200	N 47° 36'	W 103° 33'
104	Riachao Ring	Brazil	4.5	<200	S 7° 43'	W 46° 39'
105	Ries	Germany	24	15	N 48° 53'	E 10° 37'
106	Rio Cuarto	Argentina	4.5	<0.100	S 30° 52'	W 64° 14'
107	Rochechouart	France	23	186	N 45° 50'	E 0° 56'
108	Roter Kamm	Namibia	2.5	3.7	S 27° 46'	E 16° 18'
109	Rotmistrovka	Ukraine	2.7	140	N 49° 0'	E 32° 0'
110	Sääksjärvi	Finland	6	560	N 61° 24'	E 22° 24'
111	Saint Martin	Manitoba, Canada	40	220	N 51° 47'	W 98° 32'
112	Serpent Mound	Ohio, USA	8	<320	N 39° 2'	W 83° 24'
113	Serra da Cangalha	Brazil	12	<300	S 8° 5'	W 46° 52'
114	Shunak	Kazakhstan	3.1	12	N 47° 12'	E 72° 42'
115	Sierra Madera	Texas, USA	13	<100	N 30° 36'	W 102° 55'
116	Sikhote Alin	Russia	0.03	0	N 46° 7'	E 134° 40'
117	Siljan	Sweden	55	368	N 61° 2'	E 14° 52'
118	Slate Islands	Ontario, Canada	30	<350	N 48° 40'	W 87° 0'
119	Sobolev	Russia	0.05	<0.001	N 46° 18'	E 138° 52'
120	Soderfjärden	Finland	5.5	600	N 62° 54'	E 21° 42'
121	Spider	Western Australia, Australia	13	>570	S 16° 44'	E 126° 5'
122	Steen River	Alberta, Canada	25	95	N 59° 30'	W 117° 38'
123	Steinheim	Germany	3.8	15	N 48° 2'	E 10° 4'
124	Strangways	Northern Territory, Australia	25	<470	S 15° 12'	E 133° 35'
125	Sudbury	Ontario, Canada	250	1 850	N 46° 36'	W 81° 11'
126	Suvasvesi N					
127	Tabun- Khara-Obo	Mongolia	1.3	> 1.8	N 44° 6'	E 109° 36'
128	Talemzane	Algeria	1.75	<3	N 33° 19'	E 4° 2'
129	Teague	Western Australia, Australia	30	1 630	S 25° 52'	E 120° 53'
130	Tenoumer	Mauritania	1.9	2.5	N 22° 55'	W 10° 24'
131	Ternovka	Ukraine	15	350	N 48° 1'	E 33° 5'
132	Tin Bider	Algeria	6	<70	N 27° 36'	E 5° 7'
133	Tookoonooka	Queensland, Australia	55	128	S 27° 0'	E 143° 0'
134	Tvaren	Sweden	2	>455	N 58° 46'	E 17° 25'
135	Upheaval Dome	Utah, USA	10	<65	N 38° 26'	W 109° 54'
136	Vargeao Dome	Brazil	12	<70	S 26° 50'	W 52° 7'
137	Veevers	Western Australia, Australia	0.08	<1	S 22° 58'	E 125° 22'
138	Vepriai	Lithuania	8	160	N 54° 1'	E 24° 34'
139	Vredefort	RSA	300	2 018	S 27° 0'	E 27° 30'
140	Wabar	Saudi Arabia	0.1	0.01	N 21° 30'	E 50° 28'
141	Wanapitei Lake	Ontario, Canada	7.5	37	N 46° 45'	W 80° 45'
142	Wells Creek	Tennessee, USA	12	200	N 36° 23'	W 87° 40'
143	West Hawk Lake	Manitoba, Canada	2.44	100	N 49° 46'	W 95° 11'
144	Wolfe Creek	Western Australia, Australia	0.88	<0.3	S 19° 18'	E 127° 46'
145	Zapadnaya	Ukraine	4	115	N 49° 44'	E 29° 0'
146	Zeleny Gai	Ukraine	2.5	120	N 48° 42'	E 32° 54'
147	Zhamanshin	Kazakhstan	13.5	0.9	N 48° 20'	E 60° 58'

Table 1. Vrána (1987) found a circular structure in southern Bohemia between České Budějovice and Soběslav, with Ševětín near the center. Detailed study provided further evidence supporting the impact origin: shatter cones in several rock types in the central part of the structure, PDFs in quartz grains, and silicified (impact) breccia. Based on morphology and geophysical research the diameter of the whole complex structure was estimated to 46 km and diameter of the central uplift to 23 km. The chemistry of eight pyroxene microdiorite dikes from the Ševětín structure (Vrána et al. 1993) resembles impactites from the Ries crater and the character of observed contamination by Mg-Ni-Cr-rich component, might correspond to the signature of an enstatite achondrite impactor. Quartz grains containing PDFs (or PDF-like structures) from the Ševětín structure and another circular structure near Sušice (50 km in diameter) were studied using TEM, however, the microstructures observed do not correspond to shock deformations known from quartz grains from proven impact craters (Cordier et al. 1994). Nevertheless, because of deep erosion (up to more than 3 km, Vrána pers. comm.) taking place after both structures were formed the features observed now represent in fact very low levels of the original structures, so strong evidence cannot be presented to support an impact origin of both structures.

Rajlich (1992) when testing the hypothesis of Papagiannis (1989) that the Bohemian Massif is one large impact crater 260 km in diameter found in the Upper Proterozoic rock sequences of black recrystallized glasses in an area of about 1 km<sup>2</sup> underlain by breccias and/or conglomerates consisting of clasts of local origin cemented by a matrix of the identical chemistry and occurring in an area of several tens km<sup>2</sup> (probably representing an impact melt and the rocks themselves can be considered as original pseudotachylites or suevites). The idea of the astrobleme is, according to Rajlich (1992), supported not only by the finding of the mentioned recrystallized glassy-bearing rocks but also by geomorphology, the direction of water courses and geological constrains applied on the younger sedimentary covers and tectonic system. However, I find that the evidence mentioned is rather weak. The extent of the impact structure of the Precambrian age spreading over the entire Czech portion of the Bohemian Massif has not been proven yet. However, the possibility of finding remnants of the Upper Proterozoic impactites somewhere in this area in the future, cannot be excluded.

## History and development of impact hypothesis

Impact hypothesis, describing events hardly believable for most of the population, was for last century, even when meteorite falls were witnessed, an unacceptable explanation for the crater formation. Therefore, from the historic point of view, it is very interesting to trace the individual opinions of many world renowned scientists concerning meteorite falls, cratering and related effects over several past centuries because, in fact, the origin of meteorite craters during the process involving a celestial body striking the Earth was only widely accepted as late as in the second half of the twentieth century. The story of the impact hypothesis acceptance by a gradually increasing geological and astronomical community is well described in detail chiefly in articles and/or books by Marvin (1990, 1992, 1994) and Melosh (1989) (such a historical review in Czech was published by Skála (1994)).

The history of modern geology was for the last two centuries closely connected to two rather different trends explaining all geological events and the geological community was consequently divided into uniformitarians and catastrophists. The former group represented by James Hutton (1726 - 1797) and chiefly Charles Lyell (1797 - 1875) had accentuated the predominant role of slow subsequent events such as we can observe in operation now taking place at the uniform intensity and uniform rate throughout the whole geological history and rapid actions like earthquakes and volcanic eruptions had been considered as insignificant phenomena with small and local importance only. On the other hand, catastrophists (mainly Professor Abraham Gottlob Werner - 1750 - 1817) believed that all changes in the geological record had occurred due to sudden and intensively proceeding events of short duration interchanged by relatively long quiet periods.

As the hypervelocity impact of an extraterrestrial body is (fortunately) a very extraordinary event and most famous geologist in the last century believed in uniformitarian principles, pioneering opinions of German lawyer Ernst F. F. Chladni (1756 - 1827) from 1794, who, based on witnessed meteorite falls, postulated that meteorites are bodies coming from outer space caught by the Earth

gravity field, contravened the common theories ruling then. These assumed that (a) fragments of stones or irons do not fall from the skies or if they do so then they were formed by condensation processes in the atmosphere, and (b) there are no bodies in outer space behind the Moon trajectory. Although in the period 1794 - 1803 there occurred further eight well documented meteorite falls and chemical analyses of collected samples showed undoubtedly that the chemistry of meteorites is distinct from terrestrial rocks, still almost nobody from the scientific community believed Chladni's hypotheses describing meteorites as fragments of space material. Scientists rather supposed that meteorites formed in the atmosphere or came from lunar volcanoes (Marvin 1990, 1994).

Even after the acceptance of meteorites as the fragments of extraterrestrial material, there was nobody among geologists, astronomers and planetologists who thought that meteorites (or asteroids and/or comets) could play a significant role during the forming of planetary surfaces though the Moon offers numerous scars of such origin on its surface. When in 1873 an English astronomer Richard A. Proctor published his opinion that Moon craters might be the products of the "splash of meteoritic rain" he was criticized instantly by many scientists. In the second edition of his book printed in 1878 Proctor in reaction to this critique deleted the reference to the impact origin of the Moon craters (Marvin 1990).

In the seventies of 19th century, the first settlers had arrived in the region of plains in Northern Arizona. These men frequently found around the bowl-shaped depression with a diameter of about 1.2 km and depth over 170 m, called in those times, Crater Mountain or Coone Butte and located between the towns Winslow and Flagstaff, pieces of iron of various dimensions and weights. These farmers used some of them for various purposes on their farms. In 1891, it was recognized that this iron represented fragments of iron meteorite and A. E. Foote collected in the crater vicinity a total of 137 meteorites in a period of a few days. As it could be inferred from Foote's correspondence, he assumed after his field trip to the crater that the crater was produced by the collision of the Earth with a giant iron meteorite. Extremely important from the point of view of the future development of impact hypothesis are two of Foote's finds. He extracted tiny diamonds from meteoritic iron and also noted that there were no traces of lava, obsidian or other volcanic phenomena (Nininger 1956).

In the same year that Foote visited the crater, the Head of present USGS - Grove Karl Gilbert, famous and world renowned geologist and amateur astronomer interested mainly in observing the surface of the Moon - heard of the crater in Arizona. As Nininger (1956) wrote, Gilbert sent his coworker - W.D. Johnson - to visit the crater. This geologist suggested that the crater originated during the explosion of a body of warm steam formed from volcanic heat in the depth of several hundreds or thousands feet. Gilbert was not satisfied with this explanation and a year later visited the site personally and made some basic research including detailed geomorphologic study (Nininger 1956, Burke 1986). The result of the geomorphologic studies was a topographical contour map with 20 feet contour intervals (Fig. 2) and a plastic model of the crater which were used to compute accurate dimensions and volume of the cavity and the surrounding crater rim. In 1893, Gilbert wrote a paper dealing with the origin of the lunar craters, where an impact origin was preferred over a volcanic one. Although at first convinced by the impact origin of Coon Butte, Gilbert on the basis of magnetic observations (magnetic needle of the compass used was not sufficiently sensitive to detect small pieces of iron dispersed around within the crater) and volume calculations for the crater cavity and rim (both having volume of 82 million cubic yards in the contrast with Gilbert original working hypothesis that the iron projectile buried beneath the floor of the crater push the excessive matter out of the crater resulting in greater volume of the rim compared to the cavity) finally in 1896 concluded that the crater was formed by the explosion of the steam derived from the close volcanic San Francisco system. Marvin (1990) pointed out that Gilbert's opinion of excessive matter in the rim is correct, however it is valid for new impact structures only and not for those where significant denudation reduced the rim volume. Unfortunately, Gilbert's authority among the geological community worldwide meant that the impact hypothesis was for a long time considered as wishful thinking rather than a working hypothesis (using French's (1990) terminology).

Further history of Coon Butte has been closely connected to the Barringer family - recent owner of the property around the crater. Daniel Moreau Barringer - owner of a silver mine in Pearce in Arizona - heard of the crater and large amount of iron in the vicinity in 1902. Soon after he set up the mining firm (the Standard Iron Company) and obtained from the US authorities both property

and permission to explore and exploit iron from the crater. For the following almost three decades Barringer was devoted to extensive research and prospecting within and around the crater. His research brought many important finds defending the impact origin of the Meteor Crater. In 1905, the early results of this research were published. Aside from the distribution of meteorites and finds of magnetic and nickel-containing spherules inside the crater, Barringer noticed powdered silica from the crater. He concluded that the only process capable of making the crater with no radial fractures in the close vicinity, ejecting off only the thin layer of the superficial parts of the Earth crust, and grounding a silica into a powder is the impact of huge meteorite. Seeking for "iron-nickel treasure" beneath the crater floor cost Barringer 120 thousand dollars with no economic benefit. Barringer died of a stroke in 1929 shortly after publishing of a computation of the renowned mathematician, Forest R. Moulton, who discovered that the main mass of meteorite evaporated during impact and therefore within and around the crater there are only remnants of the original projectile with no commercial value (Nininger 1956, Burke 1986, Melosh 1989). Finally, Coon Butte or the Crater Mountain was renamed as the Meteor Crater and later on to the Barringer Crater to honor Daniel M. Barringer's contribution to scientific research of the site.

After the discovery of the Meteor Crater in Arizona at the end of 19th century, several other impact structures were found at the beginning of 20th century. In 1904, E. Werner described the

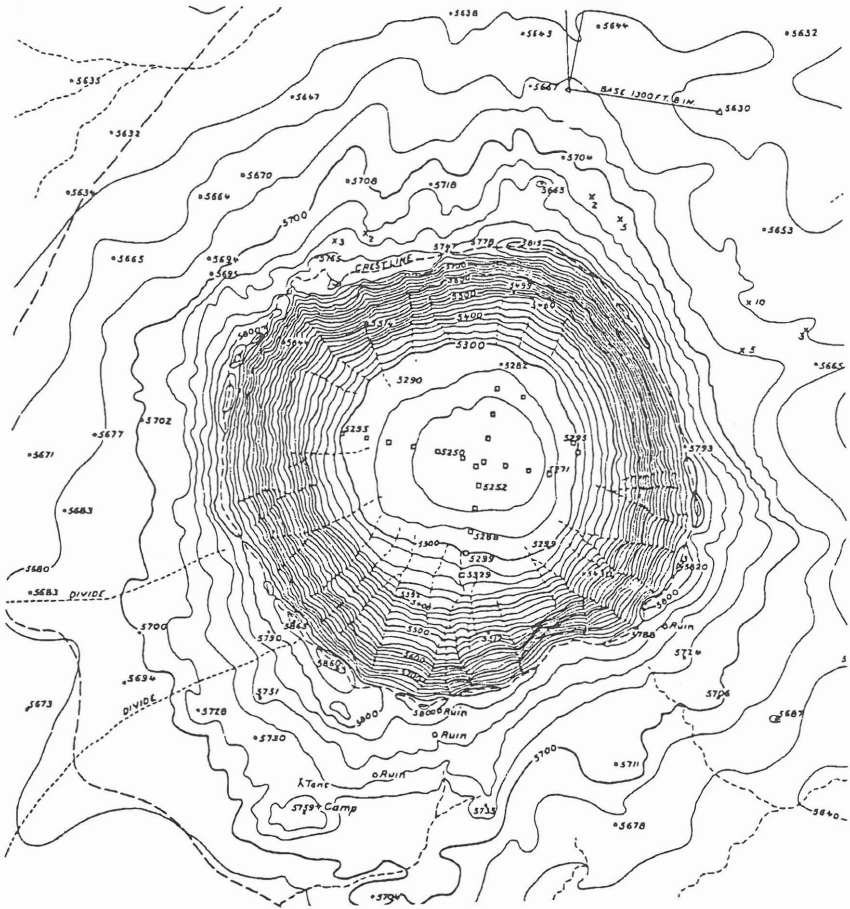


Fig. 2. Contour line map of the Barringer (Meteor) Crater in Arizona constructed by G. K. Gilbert at the end of 19th century. (After Nininger 1956).

Steinheim crater in southern Germany as the place of possible collision of the Earth with an extraterrestrial body. A year later, special conic striated features in limestones - shatter cones - were reported by W. Branco and E. Fraas who attributed their origin as well as the origin of the whole Steinheim Basin to the, up to now unknown process, "cryptovolcanism" which causes extensive fracturing of rocks without ejection of either lava or ash. The impact process in action was demonstrated in 1908 in the region of Tunguska in Russia, where, during a bolide explosion, extensive devastation of large forest areas occurred. This was an important event for further consideration of impacting as a geological phenomenon. D.M. Barringer Jr. identified a meteorite crater near the city Odessa in Texas in 1928. The crater diameter was 160 m and depth 6 m and like in the case of the Meteor Crater in Arizona there were found fragments of iron meteorite and so-called iron shale (clayish rock with high contents of iron, nickel and cobalt - Burke 1986). H.H. Nininger in 1929 discovered and in 1933 uncovered the impact structure near Haviland in Kansas with dimensions 36 × 56 feet accompanied by a few iron fragments (Nininger 1956). The aforementioned finds were followed by Alderman's discovery of 13 craters and hundreds of pieces of meteoritic iron near Henbury in Australia in 1932 (Marvin 1990). Burke (1986) noticed H. St. John Philby's find of two craters rimmed by black silica glass containing countless tiny Fe-Ni spherical features near Wabar in Arabia in the same year that the Henbury craters were discovered and pointed out that the review article of Leonard J. Spencer of the British Natural History Museum which appeared in 1933 and summarized data on known or expected impact sites (Meteor Crater, Wabar, Henbury, Campo del Cielo in Argentina, Lake Bosumtwi in Ghana, and Kaalijärvi in Estonia) played a very important role in considering and later accepting the impact hypothesis.

French's (1990) excellent article "25 years of impact-volcanic controversy" has clearly revealed the recent worldwide acceptance of the impact process as an important geological phenomenon and the development of controversy between two ways of explaining the origin of impact craters - impact hypothesis and cryptovolcanism, respectively - in the last three decades. As stated by French (1990), finding the starting point of the contention both in time and space is easy - clearly this is the Barringer (Meteor) Crater in Arizona - probably the most famous and known impact structure worldwide. This place is a well developed example of the result of a collision between the Earth and a celestial body, and the changes induced by this collision in the target materials there were observed much earlier than the impact process itself became well understood. Fragments of Coconino sandstone ejected off the crater show a whole range of shock effects from normal detritic texture, strong fracturing and crushing, intense deformation of quartz grains, resulting in cleavage and basal deformation lamellae, and complete fusion of sandstone producing vesicular pumice-like rock containing 95% silica. Moreover, the Barringer Crater samples of shocked Coconino sandstone provided the first natural finds of two hyperbaric silica polymorphs: coesite (Chao et al. 1960) and stishovite (Chao et al. 1962). Rieskessel or the Ries Crater in Germany gave not only coesite and stishovite but there were observed planar features in quartz and feldspars, transformation of tectosilicates into glassy phases without melting (so-called diaplectic or thetomorphic glasses), zircon decomposition, and pure silica glass (lechatelierite) as well.

French (1990) also noticed that several scientists defended their opinions on the terrestrial origin of impact structures even after the description of coesite and stishovite from these structures, although these minerals represent silica polymorphs formed under very specific conditions characterized by extremely high pressure pulse followed by a short period of increased post-shocked temperature and rapid quenching. The most significant person among cryptovolcanists was the American geologist Walter H. Bucher who proposed the term cryptovolcanic structure in 1936 and to his death in 1964 argued for his cryptovolcanic hypothesis (even for the Barringer Crater).

The most important part of the French (1990) article seems to be the description of a chain of scientifically logical arguments leading to the setting up of an Impact Working Hypothesis by 1968. This is based on field and laboratory observations and laboratory modeling as well. Individual aspects of the chain of evidence follow:

(a) Terrestrial impact structures exist. Evidence: Meteor Crater and other terrestrial and extraterrestrial impact structures.

(b) Impacts produce intense shock waves. Evidence: theoretical observations, analog experiments.

(c) Shock waves generate unique, long-lasting deformation effects in target rocks and their constituting minerals. Evidence: shock experiments, occurrence of such effects (e.g. shatter cones,

stishovite, shock lamellae, diaplectic glasses, increased content of Ir, Ni, Co etc. representing chemical traces of extraterrestrial impactor in target material within and in close vicinity of the structure) in known impact structures.

(d) Shock waves also produce non-unique geological phenomena that are abnormal enough to strongly support impact origin of some structures. Examples: coesite, high-temperature melting, occurrence of lechatelierite.

(e) There is no other natural process (tectonic movements, volcanism etc.) able to produce a complex of these phenomena.

(f) Finds of the above mentioned effects even in very large or old structures uniquely indicate the action of meteorite or comet impact.

At the end of his paper French (1990) proposes to “demote cryptovolcanism from its status as a Working Hypothesis to the lower category of Wishful Thinking”. His opinion is strongly supported by the increasing number of known terrestrial impact structures, finds of hyperbaric phases associated with circular structures (except for coesite and stishovite, diamond, lonsdaleite and chaoite were found to be present in shocked lithologies). The enlargement of the diameter of the Earth’s largest known impact structure, and identification of target material blocks up to 30 cm in diameter ejected from the crater to a distance more than 500 km.

Though there is a clear and consistent chain of scientifically logical arguments, several authors still try to revitalize cryptovolcanic and/or tectonic hypotheses to explain the origin of some terrestrial impact structures. These suggestions are usually based on a limited amount of evidence, e.g. just on morphology, presence of certain mineral assemblage or even one mineral, analogy to certain geochemically specific process. For example, Kopecký (1993) used the finding of armalcolite in the suevitic breccia in the Ries structure and its equilibrium pT-conditions to ascribe its origin (together with that of moldavites) to cryptovolcanism. Similarly, discoveries of the high Ir content in airborne particles from the Kilauea volcano in Hawaii (Zoller et al. 1983) and “shock-like” mosaicism in plagioclase from the Toba crater in Sumatra (Carter et al. 1986) led several scientists to the assumption that Deccan volcanism had caused K/T extinctions (detail discussion of aspects of this theory can be found e.g. in McLaren and Goodfellow 1990). However, Ar-Ar dating of the Deccan basalts revealed its age to be near to but clearly different from that of K/T boundary. Moreover, recent analytical techniques allow much effective research and shift scales of the objects studied to much smaller dimensions. Thus, hyperbaric silica polymorph coesite was described in the last two decades from xenoliths in kimberlites (Sobolev et al. 1976, Smyth and Hatton 1977), from eclogites in central China (Okay et al. 1989, Wang et al. 1989), as an inclusion in diamonds (Sobolev et al. 1976, Meyer 1987) and pyrope in metasedimentary rocks (Chopin 1984). Explanation of possible processes leading to the preservation of coesite in such conditions is discussed in detail by Hemley et al. (1994). The present author would like therefore to stress that only



Fig. 3. A view of the rim of the Barringer (Meteor) Crater in Arizona from the road between Winslow and Flagstaff.

a careful and complex study of any structure worldwide can probably solve the problem of its origin unambiguously. This can be demonstrated on other extremes where the presence of an impact structure is inferred by morphology only. For example, Papagiannis (1989), based on the Meteosat (meteorological satellite) photos only, considers the Czech part of the Bohemian Massif with boundary mountains representing an “elevated crater rim” as an impact crater of  $300 \times 250$  km dimension, and similarly, Chan and others (1992) suggest impact origin for Hong Kong from its morphology and K-Ar age determination.

## Impact craters, their morphological features and formation

Impact craters or astroblemes can be divided according to their morphology to simple and complex. Simple impact structures are typical by their circular or polygonal outline (rhomboidal shape as in the case of the Barringer Crater or hexagonal in the case of the Wolf Creek crater in Australia - Bouška et al. 1987, Bouška and Vrána 1993a), bowl-shaped depression, and elevated rim as exemplified by the Barringer (Meteor) Crater in northern Arizona (Fig. 3). Moreover, the freshest structures have their uplifted rim overlain by an overturned flap of near-surface target material with inverted stratigraphy, that is in turn overlain by fallout ejecta (Grieve 1987). Drilling at many terrestrial impact structures has shown that there is a lens of both unshocked and shocked allochthonous target rocks forming a breccia under the apparent crater floor. These breccia lenses are bounded with autochthonous brecciated and fractured target material. The just mentioned autochthonous metamorphosed rocks then define a so-called true crater which is deeper and more or less parabolic in its cross section. Shock effects in autochthonous rocks induced by a propagating shock wave generated by an impacting projectile are developed only in the lower wall and beneath the floor of the true crater. Morphometric studies (Grieve 1987 and references therein) carried out on the terrestrial simple craters gave the following relations:

$$d_{ap} = 0.14 D^{1.02} \text{ and } d_{tc} = 0.29 D^{0.93}$$

where  $D$  represents the crater rim diameter,  $d_{ap}$  and  $d_{tc}$  are depths of apparent and true crater, respectively. By comparison, lunar simple impact structures are deeper, and the apparent crater depth is given as  $d_{ap} = 0.196 D^{1.01}$ , reflecting the lower gravity of the Moon. Similarly, the gravity of a host body also affects the dimension of a transient cavity described by Schmidt and Housen (1987) as

$$D_{tc} = 1.16 (\rho_p/\rho_t)^{1/3} D_p^{0.78} v_i^{0.44} g^{-0.22}$$

where  $D_{tc}$  represents the transient cavity diameter,  $\rho_p$  and  $\rho_t$  are densities of projectile and target material, respectively,  $D_p$  is a projectile diameter,  $v_i$  represents impactor velocity, and  $g$  is a gravity constant for the host body. Cross-section through typical simple crater is in Fig. 4.

Impact structures at diameters above a certain threshold (for terrestrial structures this threshold is 2 km for sedimentary and 4 km for crystalline targets, average value for lunar and Martian structures are roughly 17.5 km and 6 km in diameter, respectively, thresholds for Mercury, Ganymed and Callisto are 16 km, 13 km, and 15 km, respectively - Grieve 1987, 1990, Taylor 1982) are developed in complex form characterized by uplifted central area, exposed as a central peak and/or concentric rings formed due to gravitational instability of simple craters at larger diameters than listed thresholds. This central region of the crater is surrounded by a peripheral basin and a faulted rim area. Peripheral depression is usually in part filled by allochthonous breccia and/or annular sheet of so-called impact melt (see Fig. 5). Coherent sheets of the impact melt occur as bodies of glassy to crystallized matter with an igneous texture and containing lithic and mineral clasts in various proportions. These heterogeneous clasts are concentrated in upper and lower contacts of sheets or lens-shaped bodies of this impact melt. Volume of the impact melt is given by the equation

$$V_m = c D_{tc}^d$$

where  $V_m$  is the impact melt volume,  $D_{tc}$  expresses the transient cavity diameter, and  $c$  and  $d$  represent mathematical constants calculated from the regression (Grieve and Cintala 1992). Generally, in the same geometric and structural position as impact-melt sheets, we find breccias consisting of dominant lithic matrix, certain portion of impact melt, mineral and lithic clasts in the impact

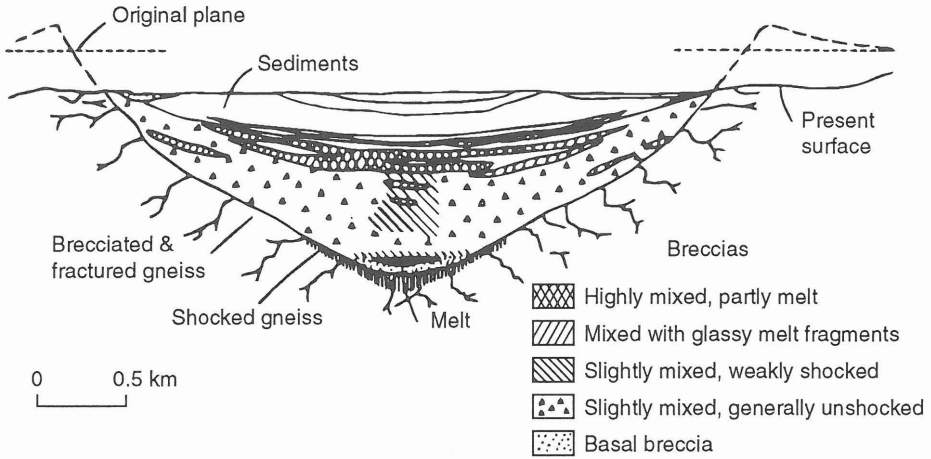


Fig. 4. Geologic cross-section of a simple crater as exemplified by Brent Crater in Ontario, Canada. (After Grieve et al. 1977 in Melosh 1989).

structures. These breccias are collectively called suevites. Shock effects in autochthonous target material are most pronounced in the rocks of the central uplifted area (Grieve 1987, Melosh 1989). Various morphological subtypes of complex craters except multiring ones were identified on the Earth including central peak craters, peak basins, peak ring basins etc. As a number of terrestrial impact complex structures is heavily and deeply eroded by later exogenic and/or endogenic processes, their topographic and morphological characteristics represent a mixture of the original structure and later topographic features now. So, simple comparison with extraterrestrial complex structures is rather problematic. However, generally it can be derived that terrestrial complex craters are shallow compared with simple ones and apparent crater depth is given by

$$d_{ap} = 0.27 D^{0.16}$$

However, as pointed out by Grive (1987), there is significant uncertainty in this equation ( $\sigma = 0.11$  on exponent) due to considerable scatter in data. Nevertheless, in general, there is an indication that the complex structures developed in sedimentary target materials are systematically shallower than those in crystalline ones.

The chief difference between simple and complex structures is the central uplifted core consisting of heavily shocked target rocks. Grieve (1987) has mentioned the formula for the estimation of structural uplift as

$$SU = 0.06 D^{1.1}$$

where SU represents the value of the structural uplift, and D is the diameter of the whole structure. The SU is defined as a net quantity of the structural uplift undergone by the deepest strata exposed now in the central area. The formula given above is based on morphometric studies at well developed complex craters allowing precise structural and stratigraphic control and represents a minimum value of the uplift, as the erosion reduces the uplift observed and an amount of the uplift decreases with depth of the structure. However, as exemplified on a structure with the diameter of 100 km, the minimum amount of the SU is roughly 9.5 km, which clearly indicate intense structural disturbance of the Earth crustal rocks in the central parts of large impact structures.

Multiring impact structures are considered either as a specific subtypes of extremely large complex astroblemes (e.g. Taylor 1982) or completely distinct type of impact produced basins (Melosh

1989). These structures have not been proven beyond doubt on the Earth yet, though e.g. Ries, West Clearwater, Manicougan, Gosses Bluff, Popigai posses multiple rings, but evidence of fluidization characteristic for extraterrestrial basins of this type is lacking (Taylor 1982). Several well developed multiring basins are found on the Moon (up to now about 40 individual structures, e.g. Mare Imbrium with the diameter of 1500 km or Mare Procellarum with diameter about 3200 km), on Mercury (basin Caloris with the diameter 1300 km), and on Callisto (basin Valhalla) (Taylor 1982). Multiring basins are characterized by the occurrence of the possible central peak ring, concentric uplifted rings at various distances from the center of the structure, and megateraces.

The process of the formation of the simple impact craters has been well understood from many

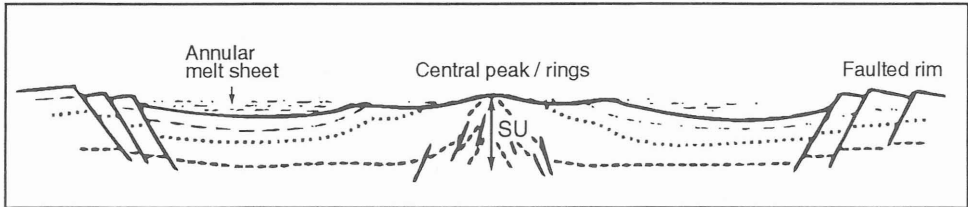


Fig. 5. Schematic cross-section of a complex crater in crystalline rocks showing the basic elements of this type of structures. (After Grieve 1987).

experimental studies, on the basis of theoretical calculations and field observations, but the model proposed to explain the origin of complex craters is in many respects controversial, as experimental modeling is not possible for such large structures (Grieve 1987, 1991). Taylor (1982) has pointed out that the formation times of impact craters are generally very short, with absolute time scales depending on the size of the structure, which is coupled with the total kinetic energy of the impactor, and therefore with its dimensions, density and velocity. Despite these short formation times, four physically different stages can be distinguished:

(1) Collision of meteorite or other projectile type, penetration and transfer of impactor kinetic energy into target material in the form of a shock wave.

(2) Shock wave rarefaction at target free surfaces, decompression of the material traversed by the compressive shock wave.

(3) Acceleration of the material by the rarefaction wave and actual excavation of the initial crater cavity.

(4) Modification of the transient crater cavity chiefly due to gravitational forces and relaxation of compressed target materials.

Depending on the crater size, the stage (1) may last fractions of a second to seconds, as typical shock wave velocities are 10 - 13 km/sec. Phases (2) and (3) overlap both in space and time and last commonly 2 to 3 orders of magnitude longer than preceding phase. Bulk ejection velocities in phase (3) are about 100 m/sec. The last - modification - stage may last for comparable time scales. So, a 10 km crater is formed within minutes, though later mild gravitational modifications can last a significantly longer period of time (Taylor 1982). Basic energy transfer takes place via the shock wave causing compression; roughly 30% of original kinetic energy is transformed into heat, 20% is responsible for fracturing and other plastic deformations in the target material, and the remaining 50% acts as kinetic energy in the form of ballistic crater ejecta transportation and displacement of target material at depth (Masaitis 1980, Taylor 1982). The shock wave is of a spherical shape and attenuates very rapidly (exponentially) with increasing distance from the point of impact due to its spherical geometry. Under these geometrical conditions the target material is affected by impact induced shock metamorphism in more or less hemi-spherical volume with strong radial pressure gradient (Stöffler 1972).

Simple crater formation process involves compression of the target rocks by a shock wave. This wave propels target material downward and outward from the point of impact. It is worth noting that the shock wave can accelerate the target rocks to velocities of a few km/sec. The shock wave

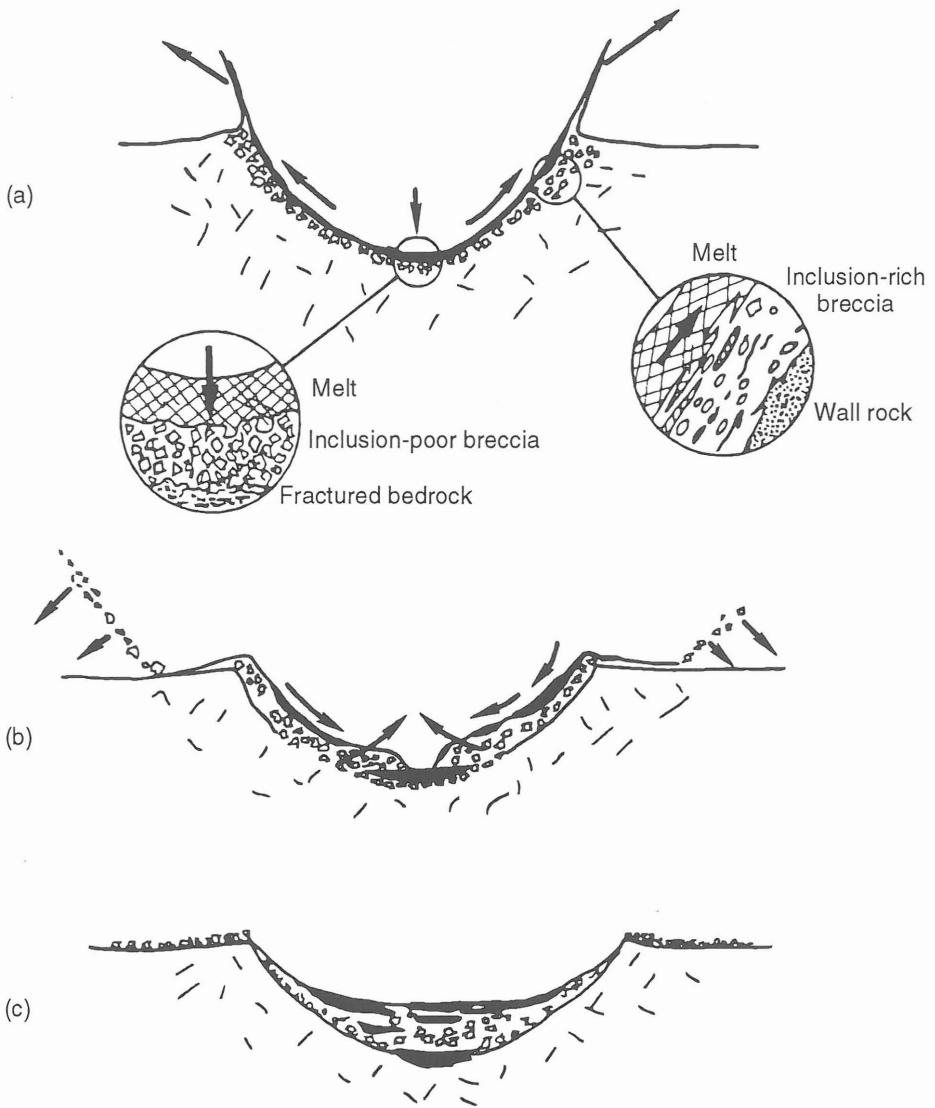


Fig. 6. The origin of a simple crater. Breccia and melt material flowing upwards along the crater walls, lines the growing transient crater (a). After the rim has been formed, breccia slides back to the crater cavity and the collapse of the transient crater begins (b). At the end of breccia sliding (c), the breccia lens becomes buried in a deep melt pocket. The remainder of the mixed breccia and melt materials that lined the transient cavity are now concentrated near the top of the breccia lens. (After Melosh 1989).

precedes the rarefaction (or release) wave which is generated at free surfaces (e.g. rear part of projectile, ground surfaces) and which decompresses the target material, and like the shock wave pushes the target material downward - directly below the point of impact. Generally, the rarefaction waves are not parallel to the compression wave, except in the region just below the impactor. Rarefaction waves thus, in most cases, overtake the target material that is moving down- and outward from the shock wave. Then the release wave interacts with these rocks and deflects some of the material upward and outward. This process ejects some of the target material from the center of the developing impact crater and altogether with the motion of the target material inside the crater downward gives rise to the formation of the initial or transient cavity (or crater), which is determined by cratering flow field and lined with fractured target rocks (Grieve 1987, 1990, 1991, Melosh 1989). The transient cavity is of a parabolic shape in a cross-section for terrestrial simple impact structures and the depth to diameter ratio ranges for this cavity between 0.33 and 0.20 (Grieve 1991 and references therein). The transient cavity is short lived and, in fact, it may never exist as a physical entity at the moment of both maximum radial excavation and maximum downward displacement. Whatever the case, the initial crater walls collapse inward extremely rapidly to form the breccia lens (allochthonous breccias), which is overlain by a thin deposit of fallback breccia that settles out of the ejecta curtain. Diagram showing the process leading to a simple crater formation is in Fig. 6.

Energetic yield necessary for the terrestrial simple crater formation can be easily exemplified by the Barringer Crater - probably the best investigated terrestrial simple impact structure yet. This scar on the Arizona plains with diameter 1200 m, depth 150 m and height of elevated crater rim 47 m was according to Grieve (1990) created by an iron meteorite of 60 m diameter and of a million metric ton mass. The meteorite collided with the Earth surface at the velocity roughly 15 km/sec and kinetic energy released due to this collision was about  $10^{17}$  J - an energy amount equivalent to the explosion of a nuclear bomb of the 20 MT TNT power. Another estimate (Taylor 1982) for the

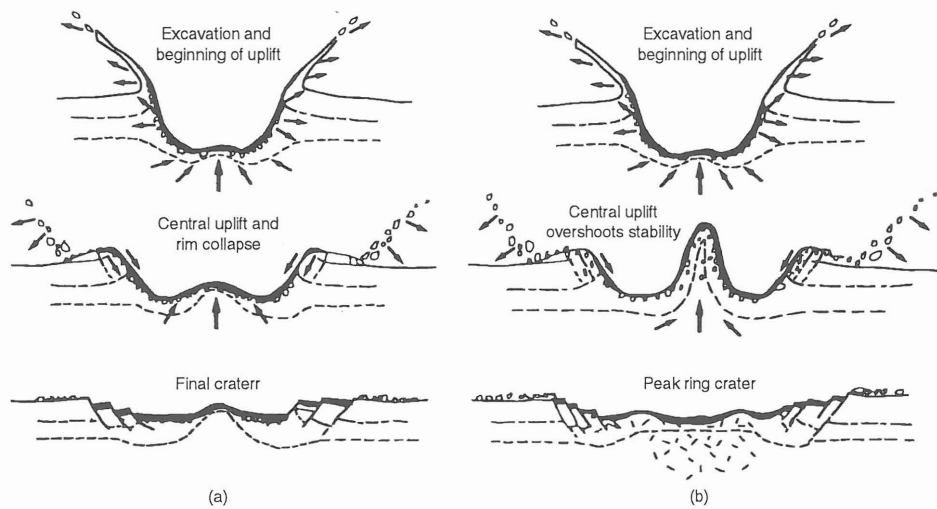


Fig. 7. Scheme of the origin of a complex crater. Part (a) shows the complex structure with a central peak, whereas a crater with peak rings is shown in part (b) of the figure. Note that uplift of the crater bottom begins before the crater rim is completely developed. Floor rise leads to crater rim collapse and formation of terraces along the crater rim. In smaller craters (a), the central uplift “freezes” and forms a central peak; in the case of larger structures (b), the central uplift collapses producing a peak ring. (After Melosh 1989).

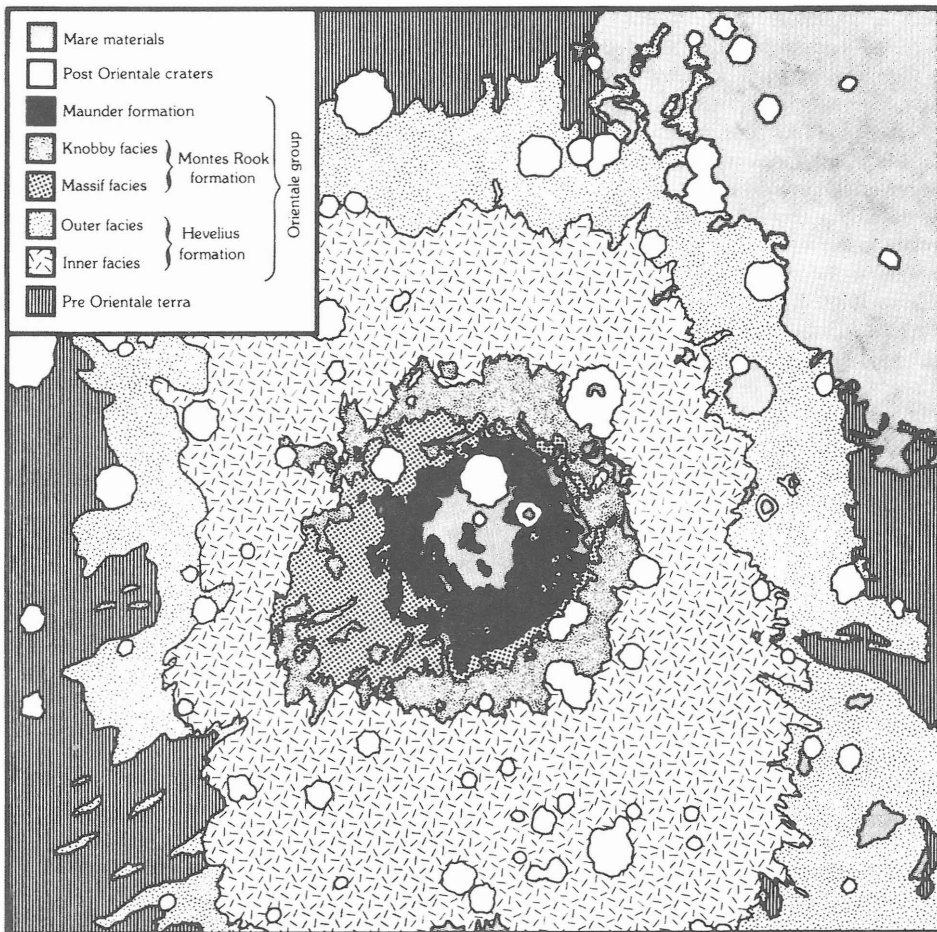


Fig. 8. Geological map of the Orientale multiring basin. (After Taylor 1982).

impacting body is that it was an iron meteorite about 30 m in diameter (some  $1.7 \times 10^8$  kg) traveling at 15 km/sec. The total energy of this projectile can be calculated as  $1.88 \times 10^{16}$  J (4.5 megaton TNT equivalent).

The complex structure develops in the initial stages as the simple one does. At the moment when the transient cavity starts to expand, some of the target materials in the center of the structure rebound upward due to the heavily changed conditions of the cratering field flow in plastic state. This upward motion in the central area lifts the floor of the initial cavity to form a central feature. After the formation of the central uplift in the form either of a simple peak or more complex features, initial crater walls and often even outer walls of the central uplifted feature slump (Grieve 1987, 1990, 1991, Melosh 1989, Taylor 1982). When the principal morphologic features of the complex impact structure are formed, further development of the formational process proceeds by the settling of the breccia from the ejecta cloud, annular sheets of the impact melt crystallization, and allocthonous suevitic breccias formation (see Fig. 7).

The formational process of large multiring basins is explained by many hypotheses whose individual stages and their sequence is sometimes rather controversial. A review of the most widely

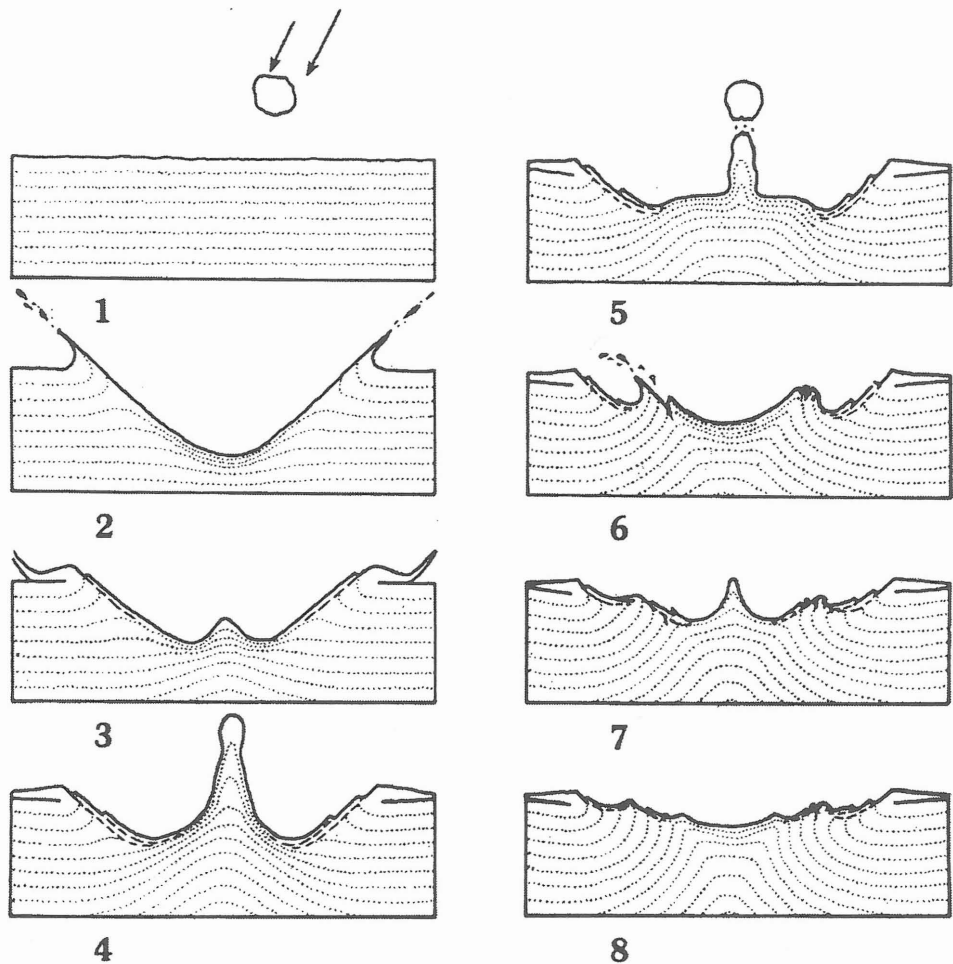


Fig. 9. The formation of the Orientale multiring basin according to the "Oscillating Peak" model. For details see text. Dashed lines indicate fractures, dotted lines represent subsurface deformations. Individual cross-sections are not to scale. (After Taylor 1982).

accepted theories is given in Taylor (1982). One of these theories - the "Oscillating Peak Theory" - set a sequence of events for Mare Orientale (for a sketch map see Fig. 8) as follows:

- (1) The initial impact causes a bowl-shaped crater 850 km in diameter.
- (2) Center area of the structure rebounds, with some slumping at the crater edge and terrace formation.
- (3) Hevelius Formation is deposited. A central mound is formed. The Cordillera Scarp reaches 920 km in diameter, through terracing.
- (4) Gravitational collapse occurs in the region of the central peak.
- (5) An inner crater (the Montes Rook ring) is formed due to collapse of the over-extended central peak.
- (6) A second rebound takes place within the Rook crater, producing another central peak, and terracing forms the Rook Mountain ring 620 km in diameter.

(7) The Inner Rook ring of the diameter of 480 km forms as a complex anticline due to collapse of the second central peak.

(8) Subsequent flooding with mare basalts at later stage causes subsidence which results in forming of the Inner Basin Scarp (320 km in diameter). Fig. 9 shows this process in diagram.

Another model, derived from the formational process of the complex structures, is based on the formation of a deep parabolic initial crater. After shock wave compression is released, the rebound in the central area of the structure occurs and the summit of the resulting central peak is significantly above the surrounding ground surface. Excavation of superficial crustal rocks at the periphery of the structure continues. The central feature becomes gravitationally unstable (due to its own weight) and almost instantaneously collapses with development of reverse faulting in the central area and excavation reaching its minimum though the impact melt and breccias are still in motion within the cavity. Peripheral parts (i.e. rim) as well the central uplift are in equilibrium height controlled by the rock strength and gravity. Excessive volume of initial central peak which cannot be accommodated by reverse faulting results in the formation of rings. At the periphery, faulting and slumping of terraces and cavity walls take place resulting in final increasing of the structure diameter like in the case of the simple craters (Taylor 1982).

### Behavior of rocks and minerals under shock compression, impactites

Impact metamorphism takes place in very distinct pressure-temperature conditions compared to those for common endo- and exogenous geological processes (see Fig. 10). Pressures during an impact event reach values several orders of magnitude higher than during endogenic processes such as e.g. eclogitization or even anatexis. Maximum post-shock temperatures achievable by impact process are also incomparable to those occurring during metamorphic or volcanic events (Bouška and Vrána 1993b, Deutsch and Schärer 1994, Grieve 1987 and 1990, Stöffler and Langenhorst 1994, etc.).

To understand processes taking place in target materials dynamically compressed by a shock

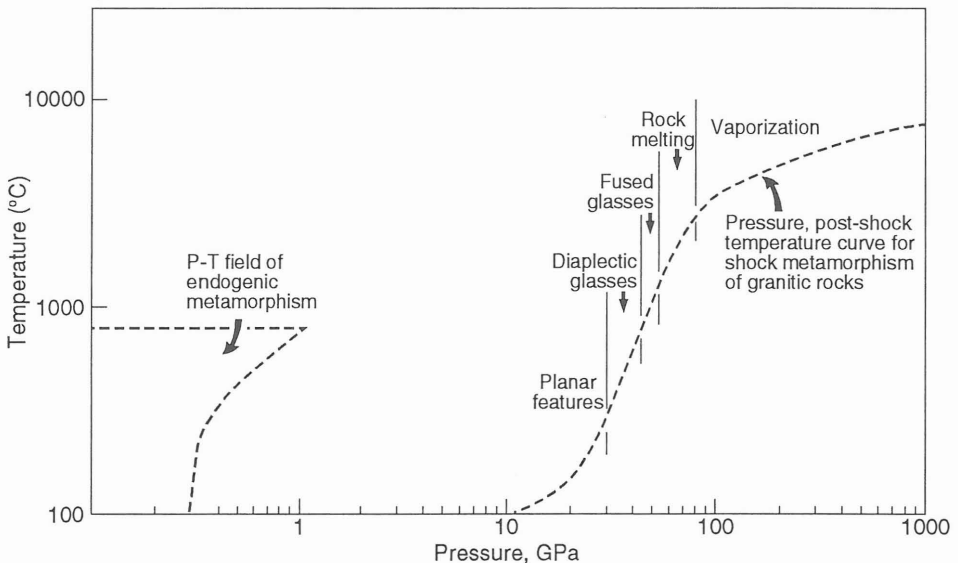


Fig. 10. Pressure-temperature field corresponding to processes during impact metamorphism in granitic rocks as compared with endogenic metamorphism. Note logarithmic scale on both axes. (After Grieve 1987).

wave it is necessary to realize the behavior of this wave. If a free plane of a solid body is suddenly highly accelerated, e.g. by an impact or chemical or nuclear explosion, a stress wave is generated. As the compressibility of solids generally decreases with increasing pressure, the stress wave becomes steeper and gives rise to a shock wave - or shock front - representing discontinuity in pressure, density and internal energy. The constituent particles are accelerated by the shock wave to a certain velocity which is behind the shock front constant. In fact, the shock wave has finite geometry and is immediately followed by a rarefaction (or relaxation or decompressing) wave traveling faster than the primary shock wave. This rarefaction wave gradually overtakes the shock one, and causes a decrease in the peak pressure and a broadening of the whole shock transition with increasing distance from the point of impact (Stöffler 1972).

For the mathematical treatment of the shock wave transition, it is useful to consider the shock wave as steady and of infinite planar geometry, connecting the initial undisturbed state with final shocked state. If we assume ideal hydrodynamic behavior of a material during the dynamic compression, we can characterize thermodynamic conditions of the shock transition by equations for mass, momentum, and energy conservation (Stöffler 1972). Consider a plane shock wave traveling at velocity of  $U$  into a solid material, which has initially both zero velocity and zero acceleration. The shock wave accelerates material and its particles after shock wave transition have velocity of  $u$ . Initial density of target material  $\rho_0$ , pressure  $P_0$  and internal energy  $E_0$  rise due to shock wave transition to values of  $\rho_1$ ,  $P_1$ , and  $E_1$ , respectively. From the conservation of mass and momentum, respectively, we get

$$\rho_0 U = \rho_1 Uu \text{ and } P_1 - P_0 = \rho_0 Uu$$

respectively, and the conservation of energy is thus expressed as

$$P_1 u = 1/2 (\rho_0 Uu^2) + \rho_0 U (E_1 - E_0).$$

Finally, eliminating of  $U$  and  $u$  by combination of relations given above we give so-called Rankine-Hugoniot equation

$$E_1 - E_0 = 1/2 (P_1 + P_0) (V_0 - V_1)$$

where  $V_i$  represents specific volume  $1/\rho_i$ . In other words, this relation describes the locus of all shock stages attainable by shock waves of various intensities in certain solid body with initial state defined by variables  $P_0$ ,  $V_0$ ,  $E_0$ . Described graphically in the diagram pressure vs. volume this locus is referred to as Hugoniot curve or simply hugoniot. This curve expressing dynamical compressibility of particular target material is specific in its shape for each type of target material reflecting its crystal structure or isotropic behavior upon compression. Other factors influencing according to Stöffler (1972) the shock wave are direction of wave propagation with respect to plane of weakness of shocked material (schistosity, cleavage, and fractures), and physical properties of this materials (e.g. viscosity, phase transitions).

The shock process, as can be easily seen in the  $pV$ -diagram, produces a certain amount of irreversible work resulting in more or less equivalent post-shock heating.

Thermodynamically, the shock compression corresponds to the Rayleigh curve and is done non-isentropically. The contrary process, due to a rarefaction wave, decompressing target material to ambient conditions, is equivalent to adiabatic one, which is isentropic. Thus, increase in entropy occurs during the impact process. Work done by shock compression is given in the  $pV$ -diagram by the area under the Rayleigh line, and energy released due to expansion corresponds to the area under adiabatic curve. Apparently, the difference between these two areas defines the residual (i.e. post-shock) heat (see Fig. 11). Upward concavity of hugoniot results in increase in entropy and therefore in post-shock heat as the peak-pressure increases. This easily explains post-shock melting and vaporization of target rocks under extremely high dynamic compression. Moreover, the post-shock temperatures are highest for materials with the largest dynamic compressibility and high porosity of original target material significantly increases residual temperatures achieved by a shock process as well (Stöffler 1972 and references therein). Residual (irreversible) changes observable in target rocks and minerals after shock compression are those formed above a certain point on the Hugoniot curve - so called dynamic or Hugoniot elastic limit (abbreviated as HEL) - which lies in the range 2 - 12 GPa for most common rock-forming minerals. With increasing peak pressure of an impact process, fracturing, cataclasis, plastic deformations, phase transitions, thermal decomposition, melting, and vaporization affect the target materials. Individual deformations caused by shock and rarefaction wave transition are specified in the following list in sequence of increasing pressure achieved by the process:

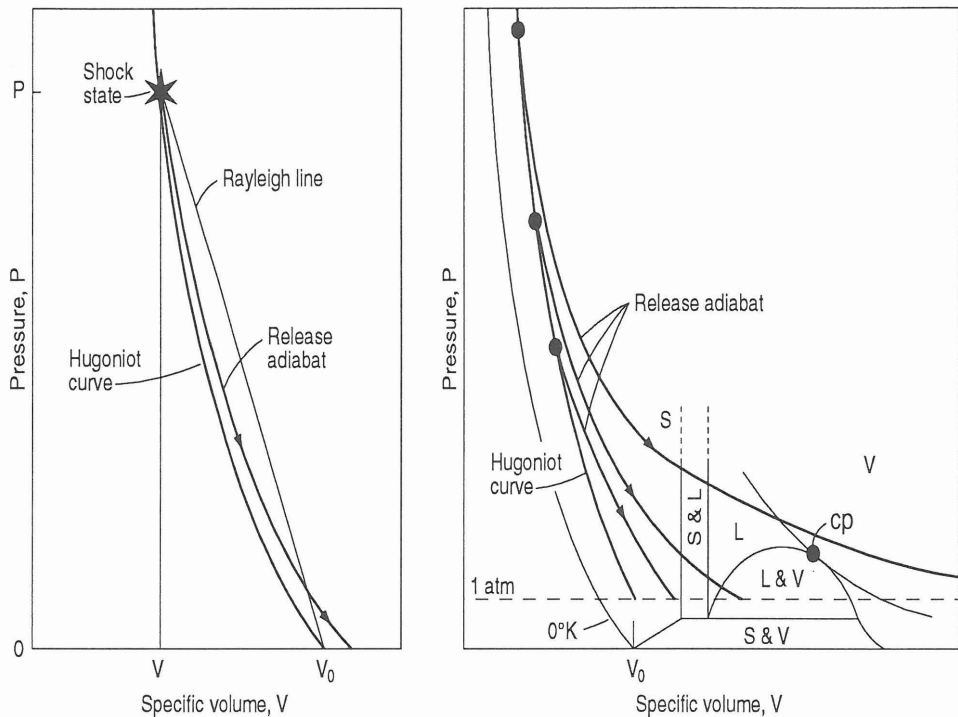


Fig. 11. Hugoniot curve, Rayleigh line and release adiabat plotted in pV-plot. (After Melosh 1989).

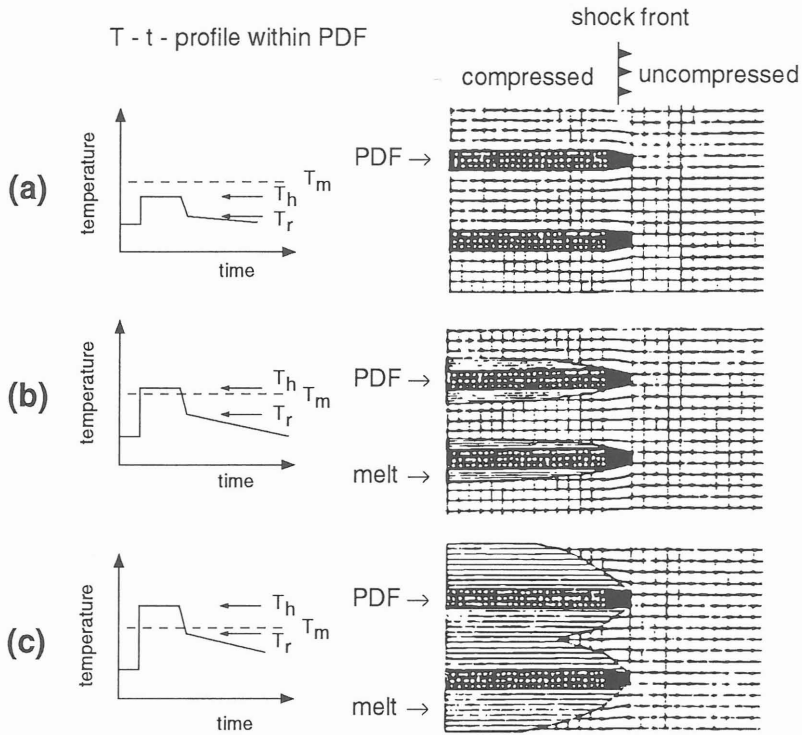
### Deformation of rock-forming minerals under shock compression

1. Fracturing
2. Plastic deformations
  - 2.1. Planar fractures (abbr. 'PF')
  - 2.2. Planar deformation features ("planar elements" - abbr. 'PDF')
    - 2.2.a. Non-decorated planar elements
    - 2.2.b. Homogenous lamellae
    - 2.2.c. Filled lamellae
    - 2.2.d. Decorated planar elements
  - 2.3. Deformation bands
    - 2.3.a. Kink bands
    - 2.3.b. Mechanical twins
    - 2.3.c. Deformation bands with diffuse boundaries ("extinction bands")
  - 2.4. Irregular plastic lattice deformation ("mosaicism")
3. Solid state transformations
  - 3.1. Phase transitions to high-pressure phases.
  - 3.2. Transition to low density, short-range-ordered phases (diaplectic glasses)
4. Thermal decomposition, melting and vaporization
  - 4.1. Shock melting.
  - 4.2. Thermal decomposition.
  - 4.3. Vaporization.

Below the HEL, fracturing and grinding may be observed in target materials due to tension

waves following after shock wave compression. Irregular fracturing is commonly found in all minerals and rocks affected by shock metamorphism over a wide range of peak pressures. Therefore, this feature cannot be used to indicate certain pressure reached by formational process. Nevertheless, the intensity of fracturing is proportional to maximum shock load and can be quantified by the fracturing index. As noticed by Stöffler, in several cases it was shown that the fracturing index is correlated with a pressure range calculated or estimated on the basis of other shock induced phenomena.

In the pressure range above the HEL, the deformations numbered as 2 - 4 in the list above originate. All PDFs are unique indicators of impact process from those. Planar fractures (PFs) occur as open fissures found in some minerals in the form of parallel sets generally oriented with crystallographic planes of low Miller indices and with spacing more than 20  $\mu\text{m}$ . They are interpreted as the microscopic results of stress relaxation behind the elastic precursor wave. In some cases, however, planar fractures cannot be distinguished from planar deformation elements. Planar deformation features (PDFs) are usually defined as multiple sets of parallel optical discontinuities sometimes resolvable under an optical microscope as thin lamellae or planes up to 2 mm thick. PDFs are generally parallel to planes with low Miller indices and their spacing within particular set ranges between 2 and 10  $\mu\text{m}$ . From the point of view of morphology Engelhardt and Bertsch (1969) distinguished in shocked quartz grains from the Ries structure four types of PDFs: non-decorated planar elements (optical discontinuities unresolvable by common optical microscope), homogeneous lamellae (lamellae with thickness resolvable by optical microscope), filled lamellae (lamellae filled with minute crystals), and decorated planar elements (optical discontinuities lined by tiny spherical to elliptical cavities). So-called decorated planar elements are products of later thermal alteration of original planar features. The origin of PDFs has been explained by several theories; the first one was presented by Engelhardt and Bertsch (1969) who considered lamellar planar features as glide planes because the most frequent orientations of these features are in directions of the shortest Burgers vectors (i.e. in those energetically favorable). Stöffler (1972) reported three possible basic processes leading to the formation of PDFs as: (1) gliding due to shear field relaxation behind the elastic wave in final stages of the shock transformation below HEL (e.g. in olivine), (2) gliding due to yielding at final shock stages above the Hugoniot elastic limit, and (3) reversion of high-pressure polymorphs to phases with short-range order (i.e. diaplectic glasses - see below) during release from shock states in the mixed-phase region (e.g. quartz and feldspars). Based on TEM studies, theoretical calculations, and shock experiments, PDFs in quartz are now interpreted as lamellae of densified amorphous material compensating lattice misfit in regions compressed by the shock wave. The formation of amorphous phase is a solid state process at lower pressures, whereas, at higher pressures, rapid quenching of melt and/or solid state transformation occur (see Fig. 12, Stöffler and Langenhorst 1994 and references therein). Deformation bands is a term used in Stöffler (1972) for all lens-, linear-, and lamellar-shaped regions occurring in crystals and having a different crystallographic orientation than that of hosts. Formational process of the deformation bands involves gliding and lattice rotations due to plastic deformation of crystals. In contrast with PDFs their basic physical and chemical properties are essentially the same as those of the host crystals. They occur as multiple sets within individual regions of  $\mu\text{m}$  to 0.1 mm dimensions and often they are not strictly crystallographically oriented. Many experiments modeling static compression have provided similar features; it is apparent that deformation bands are widely spread in many rock-forming minerals at very broad pressure regions, thus they cannot be used as pressure indicators themselves. Kink bands are a common product of dynamic compression in sheet-based structures (e.g. graphite, sheet silicates). Mechanical twins in form of polysynthetic twinning appear as sets of narrow, parallel linear to lens-shaped bands of submicroscopic to 10 mm thickness. Mechanical twins formed due to dynamic compression differ from those originating in a static regime chiefly by the crystallographic orientation of the twinning plane. Dynamically induced twins were found in pyroxenes, amphiboles, ilmenite, and titanite. Deformation bands with diffuse boundaries are commonly encountered in tectosilicates and in olivine, where they occur in the form of irregular, chiefly lens-shaped bands 0.01 mm thick. Mosaicism is defined as a highly irregular extinction pattern seen in a polarizing microscope. It represents the most common result of plastic deformation due to dynamic compression. Mutually disoriented domains and/or blocks in the crystal structure of target material are responsible for this shock induced effect forming above HEL. Altogether with PFs and PDFs mosaicism serves as an indicator of an impact event in a wide range



### FORMATION OF LECHATELLIERITE FROM SHOCKED QUARTZ

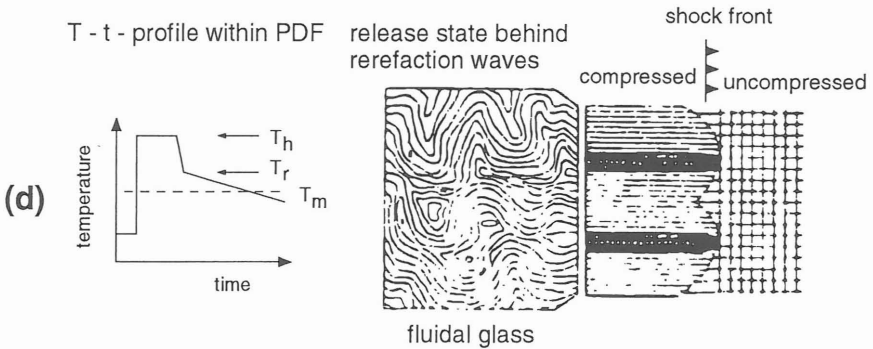


Fig. 12. Origin of planar deformation features in quartz (a, b), diaplectic glass (c), and lechatellierite (d) as proposed by Langenhorst.  $T_h$  - shock temperature,  $T_r$  - post-shock temperature, and  $T_m$  - melting temperature of quartz. (After Stöffler and Langenhorst 1994).

of peak pressures achieved by such a process. Mosaicism can be easily characterized quantitatively using shocked single crystal and a classic cylindrical film X-ray diffraction camera in both the back and front reflection regions (Fig. 13).

Solid-state transformations involve (1) phase transitions to hyperbaric phases or high-pressure phase assemblages, and (2) transitions to low density, short-range ordered phases with the same chemistry as a precursor phase. Both transitions are changes taking place at high pressure regime of the Hugoniot curve significantly above HEL. Hyperbaric phases characterized by the same chemical composition as initial phase but higher density form due to the process of dynamic compression

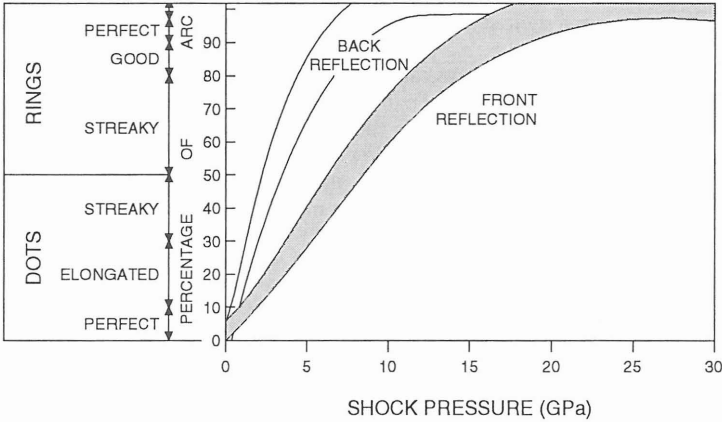


Fig. 13. Effects of shock experiments performed on quartz single crystals as observed in films using cylindrical X-ray powder diffraction camera. Note back reflections are affected by shock pressure earlier than front ones. (After Stöffler and Langenhorst 1994.)

when post-shock temperature does not exceed the melting point of the newly formed phase (e.g. coesite and stishovite at the expense of quartz, and lonsdaleite from graphite and carbon-rich substances). Most of hyperbaric phases is metastable, thus only a small portion of them remain preserved after decompression and the return of target materials to ambient (pre-impact) pressure-temperature conditions. According to Stöffler (1972) two ways lead to the formation of hyperbaric phases: (a) formation during the shock compression in high pressure regime of the Hugoniot curve (e.g. stishovite, diamond), and (b) reversion of phases of type (a) during or after the release of pressure (e.g. coesite, orthorhombic  $\text{TiO}_2$ ). Recent research based on the study of silica (Stöffler and Langenhorst 1994 and references therein) showed the principle of formation of stishovite and coesite as follows. Stishovite crystallizes during shock compression from a high pressure melt containing nuclei composed of  $[\text{SiO}_6]$  octahedra. Formational time of these nuclei is long compared to time of pressure pulse. This also explains that no more than 5% of quartz is transformed into stishovite during an impact event in silica targets; most of the high-pressure melt is quenched into diaplectic glass. Coesite, though according to equilibrium phase diagram requires lower pressure than stishovite, crystallizes from a high pressure melt, formed during shock compression, along the adiabatic decompression path of the shock transition which is broader in time compared to the peak pressure span. The kinetics of the crystallization process of coesite requires both significant overpressure ( $> 30$  GPa) compared to stishovite and long pressure pulses (in order of  $>$  milliseconds). Solid state transformation (2) leads to diaplectic (or thetomorphic) glasses. Up to now, diaplectic glasses were found to be formed at the expense of tectosilicates (e.g. quartz, feldspars). Diaplectic glasses of silica or feldspar composition appear in a polarizing microscope as isotropic grains

retaining all morphological features of the original mineral grains, i.e. grain boundaries, twin boundaries, etc. (Stöffler, 1972). Electron diffraction has shown a certain degree of long-range order compared to glass quenched from a melt resulting in two diffraction maxima at  $4.3$  and  $1.7 \times 10^{-10}$  m. The lack of these reflections in electron diffraction patterns characterizes synthetic glasses quenched from a melt (Stöffler and Langenhorst 1994). The “structure” of diaplectic glass retains a memory of the original crystalline state, so, when annealed, diaplectic silica glass recrystallizes and reverts into cristobalite or  $\alpha$ -quartz. Diaplectic glasses originate during the same pressure - temperature - time regime as PDFs do, i.e. when the temperature generated by shock wave exceeds the melting point of quartz but the post-shock temperature remains considerably below this point, the whole volume of an initial quartz crystal consists of molten PDFs (see Fig. 12). Almost instantaneously the system relaxes and temperatures drop, quenching diaplectic glass. This formation mechanism also explain the rather different properties of diaplectic silica glass and fused (normal) silica glass quenched from a melt staying above the quartz melting point for considerably longer time than a shock pulse.

When both shock and post-shock temperatures exceed melting point of target material for a certain period of time, fused (or vesiculated, i.e. normal) glasses are formed or original target materials break down into assemblage of minerals (meta)stable at new, impact generated, conditions. Hydrous minerals (kaolinite, micas etc.) break down to form anhydrous minerals or mineral assemblage. As tectosilicates tend to form glasses easily, the response of these minerals to dynamic compression is the formation of glasses quenched from a melt. These fused glasses lack any long-range ordering, reveal apparent fluidal texture showing clearly the flow of glassy matter, contain bubbles, form fillings of interstices and voids instead of retaining mineral grain boundaries as in the case of diaplectic glass. At conditions of higher temperatures the vaporization of minerals and/or rocks takes place. At certain favorable conditions vapors can condense and form vesiculated glasses and alloys after shock relaxation (e.g. the Wabar crater in Saudi Arabia).

The greatest attention in research of shock induced changes in minerals has been paid to most common rock-forming minerals - quartz and feldspars. These minerals were studied both in naturally shocked samples and those experiencing experimental dynamic compression.

Quartz ( $\text{SiO}_2$ ) has several polymorphs. In natural conditions, the most common polymorph encountered is  $\alpha$ -quartz which is stable phase below  $573$  °C; above this limit  $\alpha$ -quartz converts to  $\beta$ -quartz. High-temperature phases in equilibrium phase diagram of silica (Fig. 14) are tridymite and cristobalite, at elevated pressures (and consequently temperatures as well) coesite and stishovite are formed. During shock compression up to  $5$  GPa the fracturing occurs; these effects correspond to those observed at laboratory below HEL. Planar fractures in quartz originate at pressure range about  $5$  to  $7$  GPa or a little bit more and their crystallographic orientation is parallel to forms  $\{00.1\}$  and  $\{10.1\}$ . At higher pressures in the range  $10$  to  $20$  GPa first PDFs appear oriented parallel to mainly  $\{10.3\}$ , and at pressures  $20$  to  $30$  GPa most of lamellae are parallel to  $\{10.2\}$ ; except just mentioned orientations PDFs were found in shocked quartz grains having orientations of  $\{10.1\}$ ,  $\{00.1\}$ ,  $\{11.2\}$ ,  $\{11.1\}$ ,  $\{10.0\}$ ,  $\{11.0\}$ ,  $\{21.1\}$ ,  $\{51.1\}$  and  $\{21.1\}$ . Generally, with increasing peak pressure refractive indices and birefringence decrease. If PDFs form a dense net, anomalous biaxial behavior might be observed with the optical axial angle up to  $70^\circ$ . The same trend i.e. decrease of particular variable is known for density. On the contrary, unit-cell parameters and volume of the unit-cell increase with increasing pressure achieved by shock compression. PDFs formed at higher pressures are characterized by their wavy boundaries due to a small portion of melt originated along these boundaries at the time of maximum compression. At pressures above some  $35$  GPa the volume of this melt dominates over the volume of PDFs and melt starts to consume the whole crystal; after compression relaxation diaplectic glass is formed immediately. Aside from structural properties, diaplectic glass differs from glass quenched from a liquid by its larger density and refractive index. If quartz grains are affected by pressures from range  $12$  to  $45$  GPa, stishovite may be formed when moderately shocked rocks are rapidly cooled - this is a case of ejecta blanket or pseudotachylites or breccia dikes beneath the crater floor. Stishovite then occur as extremely fine-grained aggregates enclosed in amorphized quartz and oriented (sub)parallel to the PDFs orientation. Coesite forms fine-grained, colorless to brown polycrystalline aggregates up to  $100 - 200$   $\mu\text{m}$  embedded by diaplectic glass, or amorphized quartz with abundant PDFs. Size of coesite crystals usually does not exceed  $1$   $\mu\text{m}$ . Coesite forms at pressures  $30$  to  $60$  GPa and if it is sufficiently rapidly cooled it can be preserved in clasts of rock melts and tektites. Finally, at pres-

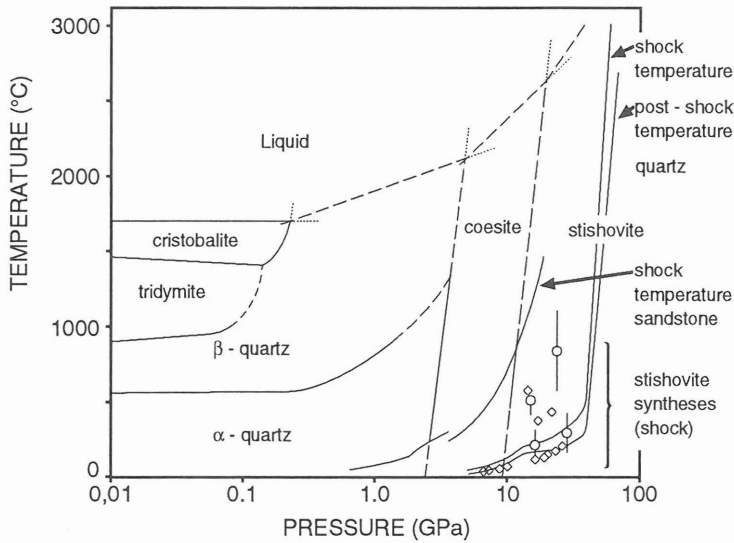


Fig. 14. Phase diagram of silica. Curves indicate shock stages during shock experiments involving single-crystals and sandstones, and circles and diamonds for syntheses of stishovite. (After Stöffler and Langenhorst 1994).

pressures above 50 GPa when both temperature generated by a shock wave and that produced by a rarefaction wave exceed the melting point of quartz, melting of quartz grains takes place and fluidal melt is formed and then after decompression quenched to form fused silica glass - lechatelierite - corresponding to cooled low-pressure melt with short-range order (Fig. 10). Finds of lechatelierite are limited only to inclusions and schlierens in rock melts, and veins and fillings of submicroscopic fissures inside quartz crystals with PDFs. This scarce occurrence of lechatelierite can be explained by the unusually extreme conditions needed for its formation (Stöffler and Langenhorst 1994).

Feldspars are generally less resistant to shock compression than quartz due to their larger dynamic compressibility. Therefore, individual effects induced by impact metamorphism appear in feldspars at lower pressure and temperature levels than corresponding effects in quartz. Planar deformation features were found in plagioclases (andesine and labradorite) at pressures between 15 and 30 GPa. Rare planar fractures were described from shocked andesine crystals; they have a similar orientation as PDFs do but probably they were formed at lower pressures. PDFs orientation in andesine grains is as following:  $\{001\}$ ,  $\{010\}$ ,  $\{100\}$ ,  $\{1\bar{2}0\}$ ,  $\{012\}$ ,  $\{130\}$ ,  $\{101\}$ ,  $\{111\}$ ,  $\{20\bar{3}\}$ ,  $\{201\}$  a  $\{1\bar{0}1\}$  (orientations  $\{131\}$ ,  $\{1\bar{0}2\}$  and  $\{1\bar{2}1\}$  were observed in one case only). Planar deformation features in labradorite were oriented along these forms:  $\{001\}$ ,  $\{010\}$ ,  $\{100\}$ ,  $\{20\bar{3}\}$ ,  $\{101\}$ ,  $\{111\}$ ,  $\{012\}$ . Although hollandite-type hyperbaric phase is expected to form from plagioclases at high pressures, this type of phase transition is not confirmed in shocked plagioclases yet. Instead of phases with the same chemistry plagioclases when subjected to pressures about 15 GPa change to metastable mineral assemblage consisting of original feldspar and newly formed jadeite. At pressures above 27 GPa diaplectic and fused vesiculated glasses start to form (plagioclase glass is frequently named as maskelynite). K-feldspar glass quenched from a melt have surprisingly higher refractive index than chemically equivalent diaplectic ones; quartz and plagioclase have the opposite trend. In all feldspars the optical axial angle decrease with increasing shock load. Plagioclases are also characterized with increasing triclinity with increasing peak pressure. The degree of shock metamorphism of plagioclases can be easily estimated from IR spectra showing in experimentally shocked minerals the gradual changes from crystalline phase to amorphous melt glass (Stöffler 1972 and 1974) see Fig. 15.

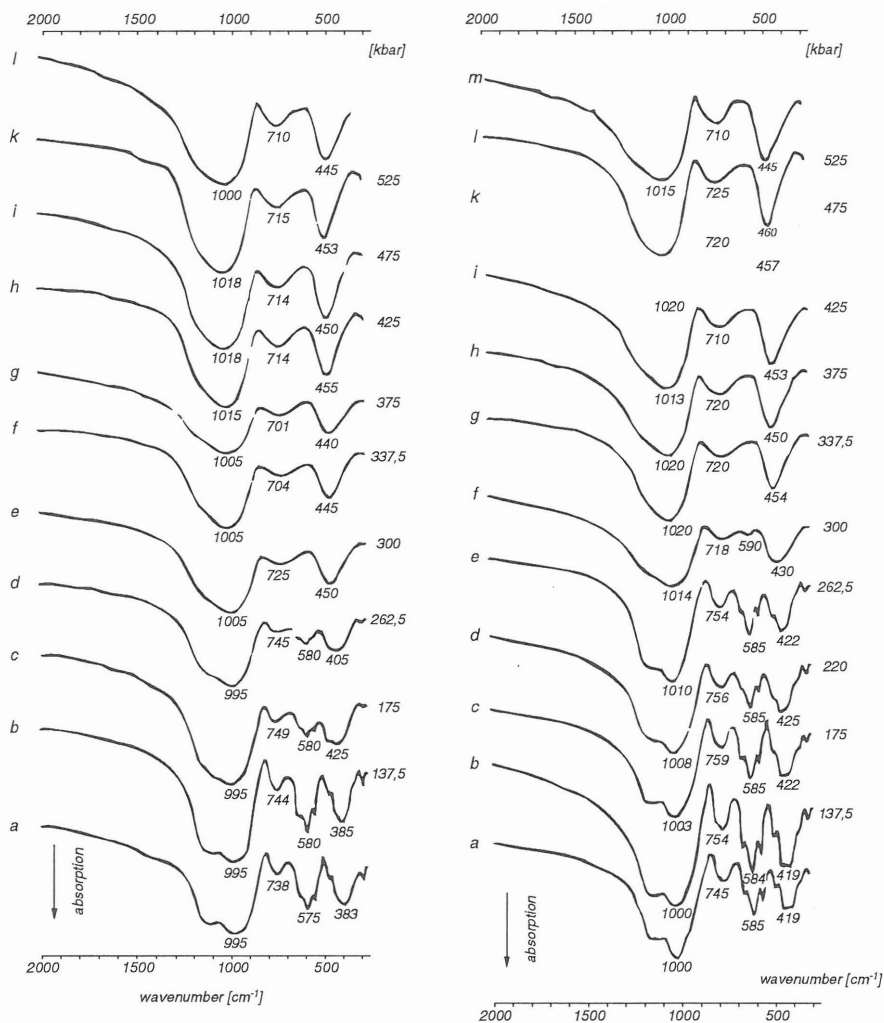


Fig. 15. Infrared absorption spectra of experimentally shocked labradorite (from Nain, Labrador) and oligoclase (from Seiland, Norway). Peak pressures are indicated for each spectrum. Curves marked with (a) correspond to unshocked standards. Uppermost spectra are for synthetic glasses. (After Stöffler, 1974).

Other rock-forming minerals such as amphiboles, micas, pyroxenes etc. when subjected to impact metamorphism also reveal some specific shock induced effects (except PFs and PDFs there were observed mechanical twins, plastic deformations, or chemical changes) which are described in detail e.g. by Stöffler (1972 and 1974). Kikuchi et al. (1993) observed the behavior of clay minerals under dynamic compression in a laboratory; kaolinite above 31 GPa lost its structure and at still higher pressures kaolinite “glass” is formed.

**Table 2. Impact induced metamorphism effects in quartz-feldspathic rocks (after Stöffler 1971, 1984).**

Shock stage	Peak pressure range (GPa)	Post-shock temperature range (°C)	Effects of shock-wave propagation
0	0 - 10	0 - 100	Fractured minerals.
I a	10 - 20	100 - 170	Quartz and feldspar grains with planar deformation features (PDF).
I b	20 - 35	170 - 300	Quartz and feldspar grains with PDFs and reduced refractive index (RI), stishovite and minor coesite.
II	35 - 45	300 - 900	Diaplectic quartz and feldspar glass, coesite and traces of stishovite, cordierite glass.
III	45 - 60	900 - 1 500	Normal feldspar glass (fused, vesiculated) and diaplectic quartz glass, coesite, cordierite glass.
IV	60 - 80 (100)	1 500 - 2 500	Rock glasses or crystallized melt rocks (quenched from liquids).
V	> 80 - 100	> 2 500	Rock glasses (melts condensed from silicate vapor).

**Table 3. Shock metamorphism effects in (ultra)mafic rocks (Stöffler, 1984).**

Shock stage	Peak(GPa) pressure (GPa)	Post-shock temperature (°C)	Observed shock effects
1	< 20 - 22.5	< 200	Fractured plagioclase, pyroxene, and olivine grains; mechanical twinning in pyroxene and ilmenite.
2	< 40 - 45	< 900 (?)	Plagioclase grains with PDFs and diaplectic plagioclase glass; twinning in pyroxene and ilmenite.
3	< 60	< 1 100 (?)	Plagioclase glass with incipient flow structure; mafic minerals as in stage 2.
4	< 80	< 1 500 (?)	Normal (fused) plagioclase glass with vesicles and flow structure; incipient edge-melting of pyroxene grains.
5	< ?	< ?	Normal plagioclase glass increasingly mixed with melt products of pyroxene and ilmenite; recrystallized olivine grains; whole rock glasses at higher pressures (about 100 GPa).
6	< ?	< ?	Rock glass condensed from silicate vapor.

According to the effects caused by the impact process in particular minerals or whole rocks in certain target materials the peak pressures and maximum post-shock temperatures achieved by this process may be inferred. Shock stages and corresponding mineral and/or rock indicators were established for common granitic rocks by Stöffler (1971, 1984), for mafic and ultramafic rocks and meteorites, respectively, also by him and co-workers (Stöffler 1984 and Stöffler et al. 1991, respectively), and for porous sandstone by Kieffer and others (1976). These metamorphic stages are summarized in Tables 2-5 and in Fig. 16.

**Table 4. Shock metamorphism of porous sandstone according to Kieffer et al. (1976) as modified by Stöffler (1984).**

Shock regime	Shock class	Pressure (GPa)	Temperature (oC)	Observed shock induced phenomena
A		< 0.2 - 0.9	< 25	Undeformed sandstone
B	1 a	< 3.0 (< 2.2 - 4.5)	< 250	Deformed sandstone with remnant porosity
C	1 b	< 5.5 < 3.6 - 13)	< 350	Deformed sandstone compressed to zero porosity
D	2	< 13	< 950	Dense sandstone with 2 - 5% coesite, 3 - 10% glass, and 80 - 95% quartz.
E	3	< 30	> 1000	Dense sandstone with 18 - 32% coesite, traces of stishovite, 0 - 20% glass, and 45 - 80% quartz.
F	4	> 30	> ?	Dense sandstone with 10 - 30% coesite, 20 - 75% glass, and 15 - 45% quartz.
	5		> ?	Vesicular rock with 0 - 5% coesite, 80 - 100% glass (lechatellierite), and 0 - 15% quartz.

Pressure values listed in the corresponding column of this table represent an equilibrium pressure, peak pressures can be significantly higher and estimates of these are given in parentheses.

**Table 5. Shock metamorphism effects in chondrites according to Stöffler et al. (1991)**

Shock stage	Criteria	Pressure (GPa)
S1	Sharp optical extinction in olivine grains.	< 4 - 5
S2	Undulatory extinction in olivine grains*.	< 5 - 10
S3	Planar fractures in olivine grains*.	< 15 - 20
S4	Mosaic extinction in olivine grains*.	< 30 - 35
S5	Plagioclase converted to maskelynite and planar deformation features in olivine grains.	< 45 - 55
S6	Solid state recrystallization in olivine grains.	> 45 - 55

\* Meteorite is assigned to this shock stage if > 25% of the olivine grains exhibit this feature.

Impactites is a collective name for rocks formed during the impact event from target materials by the action of projectile or shock and/or release waves generated by it. Crater walls, materials beneath the crater floor, impact melts, and rocks significantly transported by shock mechanism to allochthonous positions as well, reveal the most apparent effects of impact metamorphism manifested by heavily fracturing, brecciation, cataclasis, and melting (coptoclasites of Masaitis and others (1980)).

So-called shatter cones - conical striated features (Fig. 17) - represent a unique feature produced by an impact metamorphism in the pressure region 2-25 GPa. The best developed examples of shatter cones are found in fine-grained and texturally isotropic rocks (Grieve 1987). Widespread opinion assumes that apexes of shatter cones point to the place where the shock front was generated. However, several samples with shatter cones oriented in a rather random way in a relatively small area suggest that the apexes might not be used as accurate indicators of initial shock wave propagation direction; more probably they show the complicated geometry of the shock front, reflected compressive waves, and rarefaction waves as well. As stressed by Grieve (1987), although formation of shatter cones was modeled successfully in a laboratory, the physical principles of their formation are not well understood yet.

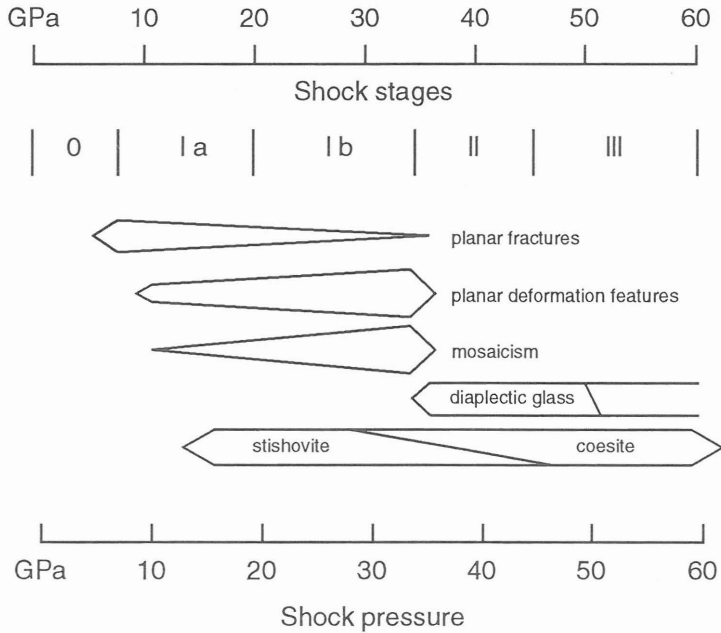


Fig. 16. Diagrammatic expression of shock stages and equivalent pressure ranges in quartz obtained from experimental data. (After Stöffler and Langenhorst 1994).

Rock types commonly in the form of dikes and consisting of fine-grained or glassy, predominantly dark matrix, sometimes retaining flow features, are known as pseudotachylites. The matrix contains clasts of rocks and minerals derived from local target material. The origin of pseudotachylites is ascribed to frictional melting due to high-speed slips (including vibrations) along slip surface (i.e. fault) or passage of a shock front through the host material (Spray 1993). Clasts in pseudotachylites occur as angular fragments (i.e. like in a breccia), but more commonly in the form of rounded or sub-rounded fragments. The thickness of pseudotachylites can vary from millimeter sized veinlets to dike-like bodies up to a kilometer thick. However, not all pseudotachylite occurrences are products of impact metamorphism. Austerheim and Boundy (1994) have described pseudotachylite veins consisting of microlites of omphacite, garnet, plagioclase, and quartz, exposed in Grenvillian granulites of the Bergen arcs in western Norway. These pseudotachylites may have formed as a result of the rapid stress relaxation during eclogitization. Nevertheless, there are many examples where pseudotachylites are clearly connected to impact structures in both place and origin. These are tiny veinlets up to 1 mm thick, which cannot be the product of any endogenous geologic process taking place along any shear zone (Spray 1993), and, moreover, contain as in the case of the Vredefort structure, hyperbaric silica polymorphs - coesite and stishovite - in form of acicular aggregates within quartz clasts (White 1992) or occur as thin melt films on surface of shatter cones (Reimold and Collinston 1992). Occurrence and character of pseudotachylite veins show that the nets of thin veins and veinlets in rock crater basement are the result of initial impact stages - forces compressing target materials and those connected to transient cavity collapse - whereas thick pseudotachylite dikes correspond to the decompressive stages of crater evolution (i.e. are products of rarefaction waves - Spray 1993, White 1992). Reimold and Collinston (1992) suggested the use of the term pseudotachylite in the non-genetic meaning since this word is widely spread over geological literature and used there, in many cases, in a rather different way. Therefore, for pseudotachylites in the impact structures, genetic terms such as a frictional melt or impact melt

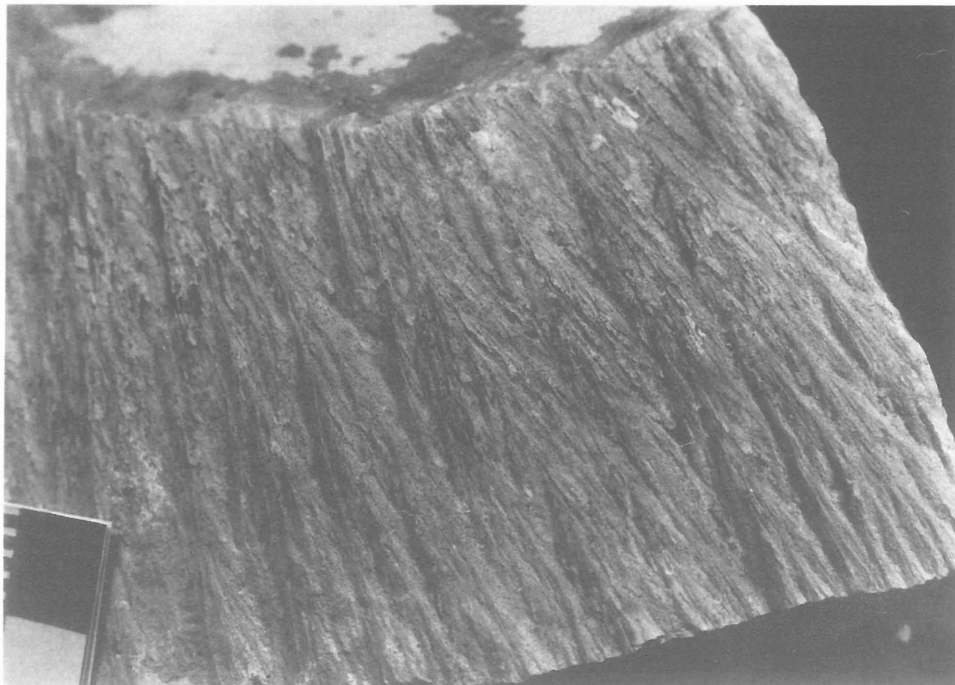


Fig. 17. Shatter cones on the surface of the Malmian limestone from the Steinheim basin in Germany.

should be used. On the other hand, Rondot (1989) has suggested using the term pseudotachylite for autochthonous breccias with dark aphanitic glassy matrix formed by partial melting of the host rock.

Rondot (1989) has also proposed naming (para)autochthonous breccia- or conglomerate-like rocks consisting of matrix derived from fractured target materials and clasts of similar composition mylolistenites. Mylolistenites differ from pseudotachylites because they do not contain glassy matter in the matrix - i.e. that derived from frictional melting - though they may accommodate glassy clasts (impact melt). As noted by Rondot (1989) mylolistenite irregular bodies or dike-like features in the impact structures reach the thickness of up to decimeters or even meters (e.g. Carswell, Charlevoix, and Siljan).

The basement beneath the crater floor, crater close vicinity, and crater walls are places where different types of breccias are encountered. They can be divided according to the origin of clasts accommodated in the matrix into autochthonous or allochthonous, and according to the character of materials forming the breccia into monomict or polymict respectively. Moreover, based on a detailed study of the boundaries of these often dike-like breccia bodies with their host rocks, the formational process giving rise to these dikes can be inferred (e.g. Müller-Mohr 1992).

Suevite (Fig. 18), a rock connected by its origin to impact structures, was first described from the Ries crater by Werner and defined by him as polymict crystalline breccia containing impact melt in different proportions. Components in these rocks reveal various stages of impact induced shock effects, however, the presence of the glass formed by melting of target materials is a characteristic feature for suevites (Chao et al. 1978). Bringemeier (1992) based on a study of new outcrops of suevite in the Ries crater near Nördlingen in Germany has confirmed Wagner's original observations that the suevite layer is divided into main suevite rich in pancake shaped bombs (so-called flädle), and relatively well-sorted thin-base suevite consisting of fine gravel and bubble-containing angular glass fragments (Fig. 19). These observations also strongly support the opinion that suevite was transported at the time of its formation in a viscous flow erosionally reworking the subsoil shifting on it.

Impact melts are found as pockets up to several meters thick in the breccia lens of simple craters, as coherent annular melt sheets reaching thicknesses up to several hundred meters surrounding the central peak area in complex structures, as glassy clasts in breccias and veins beneath the floor of impact structures, and as glassy bombs in ejecta deposits. A characteristic feature of impact melts is the high compositional homogeneity corresponding to a mixture of target rocks even in volumes of several hundreds of cubic kilometers. The other basic characteristic can be seen in significant textural inhomogeneity most apparent in melt sheets of complex structures. At the top and bottom of such an annular coherent melt sheet there are numerous lithic and mineral clast both unshocked and having experienced shock metamorphism. The clast content decreases and matrix grain size increases toward the middle part of the sheet. Clasts are removed from the melt by resorption and reaction with the matrix melt, and their population is biased to more refractory rocks and minerals (Grieve 1987 and references therein). As stated in Grieve (1987) chemical homogeneity of impact melts occurring in melt sheets can be explained by their origin as a mixture of melted and vaporized rocks propelled down to the transient cavity by a turbulent flow of high speed. Textural inhomogeneity encountered in these annular coherent impact melt sheets is caused by the incorporation and later selective destruction of clasts and by variations in post-impact cooling history, which is more or less given by the vertical position within the sheet. Obviously, impact melts are superheated liquids, so they remain liquid even when they resorb a high content of cold clasts, and due to their high temperature these melts transform usual minerals to ultra-high-temperature breakdown products (e.g. baddeleyite is formed from zircon). In some cases, the  $K_2O/Na_2O$  ratio found in impact melts is higher than that encountered in in-situ target materials. Explanation of this phenomenon is possible when either selective vaporization and condensation during melt and vapor formation or later hydrothermal alteration of felsic clasts occurred (Grieve 1987).

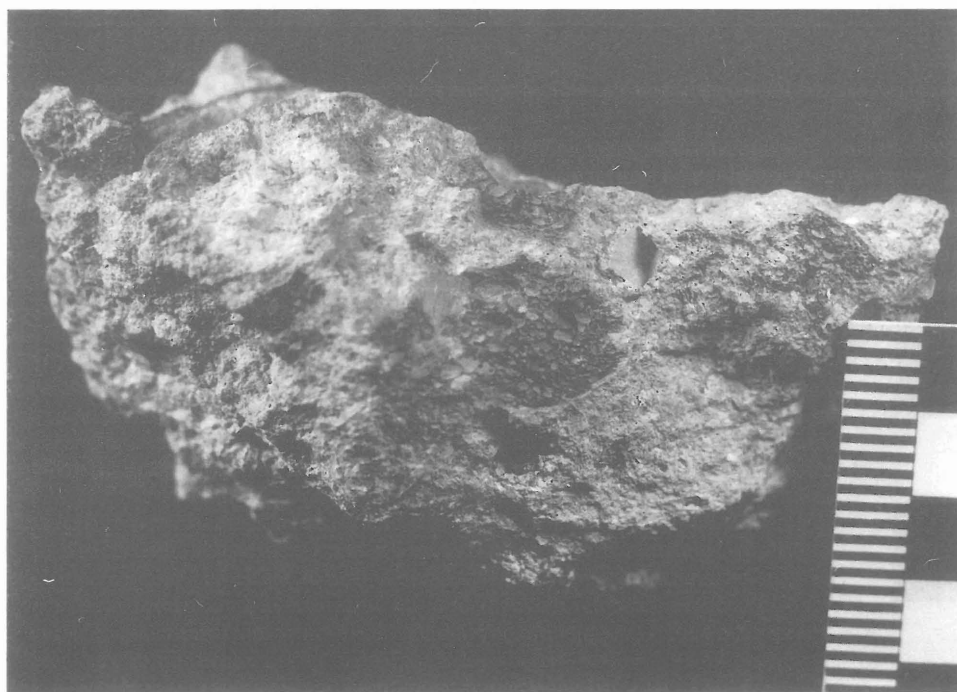


**Fig. 18.** Suevite: air fall polymict breccia containing abundant fragments of glass bombs. Matrix consists mainly of montmorillonite.

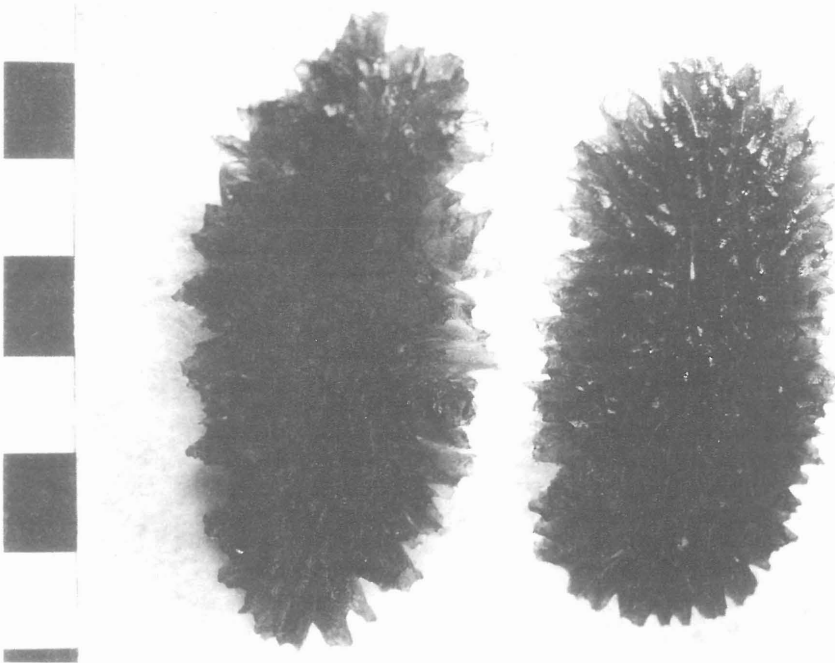
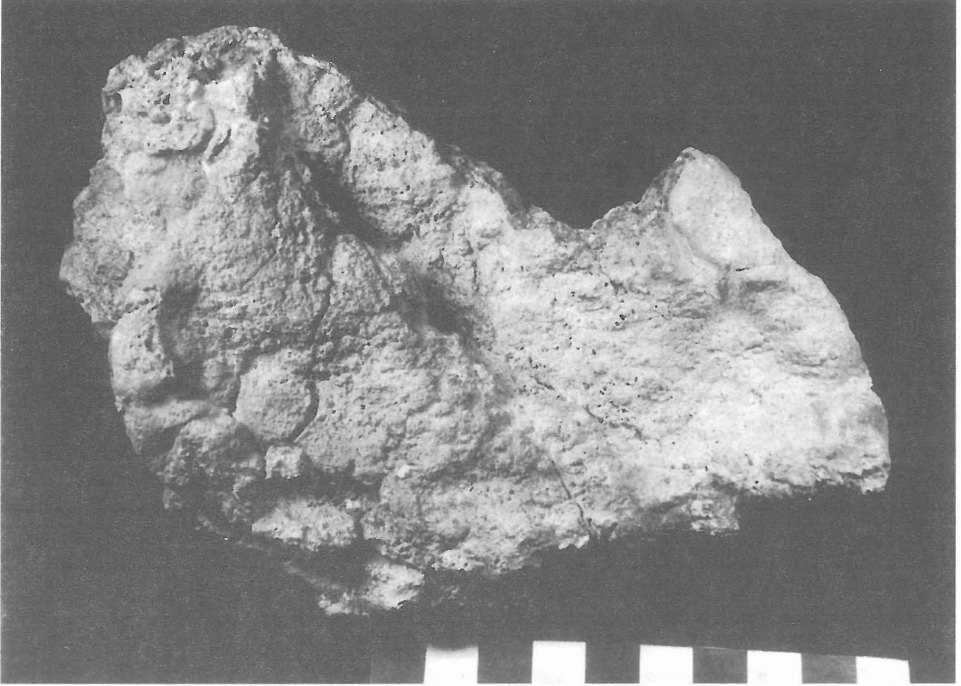


Fig. 19. Impact glasses: (a) impact glass from suevite (proximal impactite), (b) tektite (distal impactite).

Russian scientists frequently use the term tagamites for massive impactites containing larger amounts of glass (Masaitis et al. 1980, Masaitis 1992). The equivalent name used for these rocks internationally should probably be impact melts and/or pseudotachylites.

The materials ejected during the impact event into the atmosphere from a crater fall later on either back to the crater, forming a crater fill, or outside the crater rim, giving rise to an ejecta blanket. In some cases, the ejecta blanket is widely spread. Worldwide expanded ejecta are known from the K/T boundary; they are characterized chiefly by content of minerals with PDFs (quartz and zircon grains), and associated Ir and other siderophile elements enrichment. However, K/T ejecta are rather fine-grained, the only known medium- to coarse grained ejecta horizon covering a relatively large area were found in Bunyerroo Formation at many localities within the Adelaide Geosyncline and in the Lower Rodda beds of the Officer Basin in Australia (Gostin et al. 1992). Ejecta consist of angular fragments of acid volcanic rocks ranging from the fine-sand size up to 30 cm across (the boulder size) and obviously are derived from the Acraman impact structure. Gostin and others (1992) observed ejecta about 350 km NE of the Acraman structure and roughly 470 km NW of the crater. The thickness of the ejecta layer varies between 0 and 40 cm and rock types occurring within the ejecta horizon are (from base upward) breccia, sandy mudstone, and graded sand. The vertical gradation observed is attributed to settling of the ejecta in marine water column of about 200 m depth.

A proposal of impactite classification has been distributed by a Study Group on "Impactites" established by the Subcommittee on the Systematics of Metamorphic Rocks (SSMR) of the International Union of Geological Sciences (IUGS). This study group has redefined the term impactite to represent any rock affected by an impact or impacts as a result of collision or collisions of planetary bodies (Stöffler and Grieve 1994). This classification distinguishes between products of single and multiple impacts, so it allows classification of both terrestrial and extraterrestrial rocks. Two parallel sets of classification criteria were used, (1) a combination of lithological, and texture aspects, and degree of shock metamorphism as well, and (2) mode of occurrence. The recent classification proposal follows:

## I. Impactites from a single impact

### A. Classification according to components, texture and shock metamorphism

1. Shocked rocks
2. Impact melt rocks (clast-free)
  - 2.1. Glassy impact melt rocks (impact glasses)
  - 2.2. Hypocrystalline impact melt rocks
  - 2.3. (Holo)crystalline impact melt rocks
3. Impact breccias
  - 3.1. Monomict (cataclastic) impact breccias
  - 3.2. Polymict clastic impact breccias
    - 3.2.1. Fragmental impact breccias (without melt particles)
    - 3.2.2. Suevite breccias (with melt particles)
  - 3.3. Impact melt breccias (clast-bearing)
    - 3.3.1. Glassy impact melt breccias
    - 3.3.2. Hypocrystalline impact melt breccias
    - 3.3.3. (Holo)crystalline impact melt breccias

### B. Classification according to mode of occurrence

1. Massive impactites (irregular bodies, layers, lenses, blocks)
  - 1.1. Autochthonous (authigenic)
  - 1.2. Allochthonous (allogenic)
    - 1.2.1. Inside crater rim (crater fill)
    - 1.2.2. Outside crater rim (ejecta blanket)
2. Impact breccia dikes
  - 2.1. Fragmental breccia dikes

- 2.2. Suevite breccia dikes
- 2.3. Melt breccia dikes (clast-bearing impact melt)
- 2.4. Pseudotachylite (clast-bearing frictional melt)
3. Impactoclastic air fall beds
4. Tektites

## II. Impactites from multiple impacts

1. Impact regolith (unconsolidated impactoclastic debris)
2. Shock lithified impact regolith (consolidated impactoclastic debris)
  - 2.1. Regolith breccias (with matrix melt and melt particles)
  - 2.2. Fragmental breccias (without matrix melt and melt particles)

A flowchart for single impact events showing impactites classification according to both composition and mode of occurrence (Stöffler and Grieve 1994) is given in Fig. 20. Impact melt lithologies are found as allochthonous coherent sheets, inclusion in polymict impact breccias (suevite), dikes and veins in autochthonous shocked crater basement, individual melt particles ("glassy bombs") within ejecta, glass spheres in global air fall beds (distal ejecta), and tektites. Shocked rocks are defined within this classification scheme as allochthonous clasts within polymict impact breccias, impact melt rocks, and air fall beds, and as autochthonous materials of the crater basement. Terms allogenic (= allochthonous) and authigenic (= autochthonous) have the same meaning as in classic geology or sedimentary petrology, i.e. autochthonous materials are those which are not affected by any transport and remain after the impact event in their original places, on the contrary, allochthonous materials are not any more physically connected with areas of their original occurrence (all types of ejecta, breccia lens etc.). However, several researchers (e.g. Deutsch and Schärer, 1994) consider at least part of breccias beneath the crater floor as paraautochthonous materials - i.e. rocks with certain but not zero displacement.

A find of projectile remnants is one evidence of the impact origin of a particular impact structure. As can be seen in the Barringer crater history, the occurrence of meteoritic iron within the crater, in its vicinity, and even beneath the crater floor contributed to the acceptance of the impact process as geological phenomenon. The Barringer crater 1.2 km in diameter represents the biggest known terrestrial impact structure containing impactor fragments. For larger astroblemes, as noted by Grieve (1991), the deceleration of projectile was not significant resulting in such pressure-temperature conditions leading to breakdown and vaporization of impactor. Certainly, the melting and vaporization of the impactor lead in many cases to the enrichment of impact melts and breccias in several elements whose higher contents are uncommon in terrestrial materials. So, increase in contents of Cr, Ni, and Co in ppm level, and Ir in ppb level compared to the background of country rock equivalent to target materials shows an admixture of impactor component in studied rocks and in some cases the type of projectile can be inferred from the chemical pattern observed in impact melts (see Table 6). Grieve (1987) has also pointed out that the absence of detectable enrichment in siderophile elements does not necessarily mean the absence of the projectile component in shocked lithologies, since the composition of several types of impactors (e.g. basaltic achondrites, some irons, stony irons) does not allow to distinguish small admixture of the extraterrestrial component in target rocks from the unaffected terrestrial equivalents due to their compositional similarity. In case of smaller craters, on the contrary, the amount of the meteoritic component is considerably higher, so there it is possible to infer events taking place at the time of impact. For example, Mittlefehldt and others (1992) compared chemistry of impact melts in the Wabar crater in Saudi Arabia with that of iron meteorites Wabar and Nejed (so-called paired meteorites which based on their chemistry are considered to be derived from one meteoroid) and found that impact melts are enriched by siderophile elements of projectiles. Tiny spherical bodies of impact melt, that had undergone ballistic transport and that were aerodynamically shaped, contain up to 17% of meteoritic component, and massive black and white melts contain up to 5% of this component. Relative abundances of individual siderophile elements reveal complex fractionation of impactor material during projectile vaporization (due to ablation) and accommodation of impactor matter into impact melts.

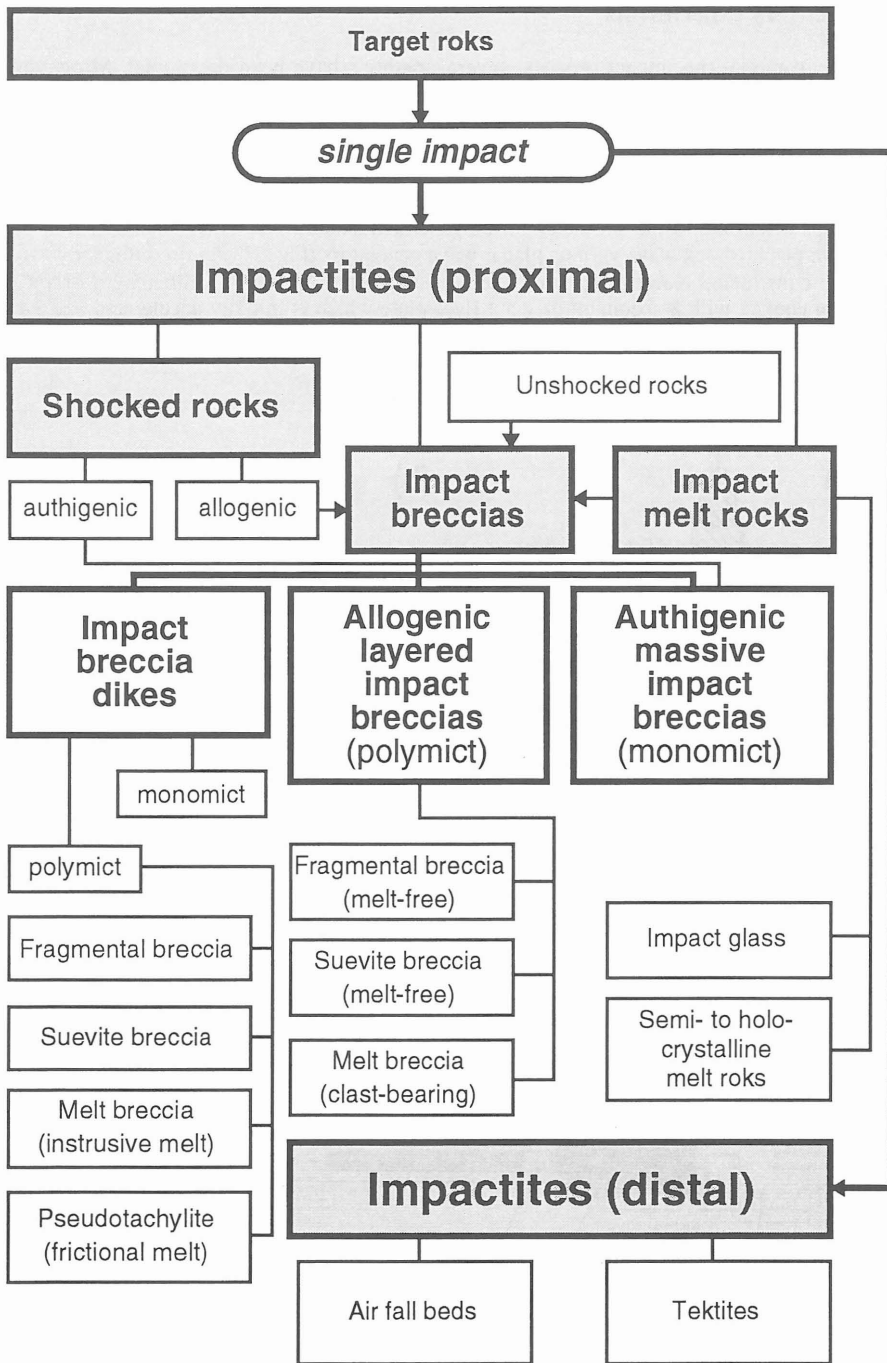


Fig. 20. Flowchart indicating the classification of impactites produced by a single impact as suggested by the Study Group on "Impactites" established by the Subcommittee on the Systematics of Metamorphic Rocks of the IUGS. (After Stöffler and Grieve 1994).

## Shock recovery experiments

In order to model the impact process, several methods have been developed. Moreover, the industrial and military explosions (of either classic or nuclear explosives, missiles, etc.) have helped to understand and explain some of the aspects of shock wave propagation and behavior of some natural and/or man-made materials under extremely high pressure dynamic compression. If we omit industrial and military tests we can focus our attention just on scientific shock wave experiments allowing to recover the shocked sample for further study. They can be divided into two basic groups according to the geometry of the generated shock front: either planar or non-planar. To generate planar shock wave various planar wave generators (Fig. 21) are used. Planar wave generators are constructed either to transmit kinetic energy into the sample either by a driver plate which is in contact with a specimen or via a flyer plate which is initially accelerated and later on impacts the specimen. The former method can achieve peak pressures in a range 10 to 150 GPa, the

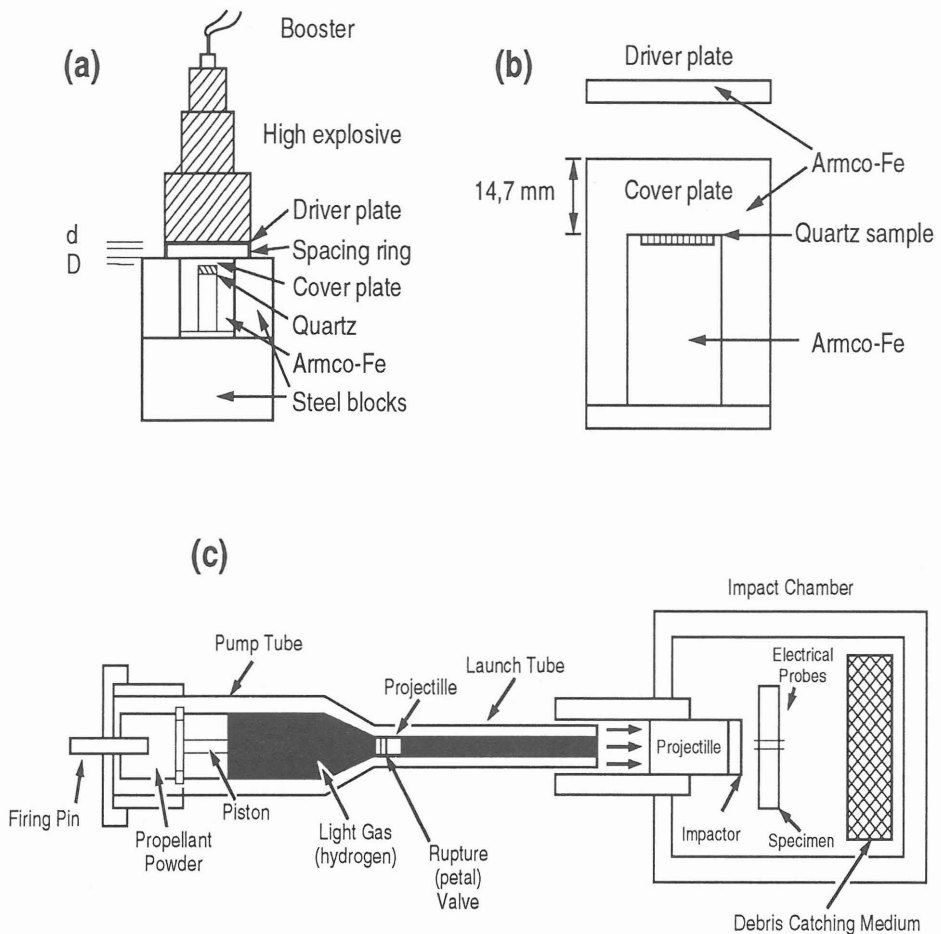


Fig. 21. Experimental set-ups for shock plane-wave generators: (a) high-explosive device used at the Ernst-Mach Institute, (b) detail of the sample container from device (a), and (c) two-stage light gas gun. (After Stöffler and Langenhorst 1994).

**Table 6. List of terrestrial impact structures with known projectile type. In upper part of the table, there are listed structures with remains of a projectile in crater or in its close vicinity, below the dashed line the projectile type is inferred only on the basis of geochemical data. [modified according to Grieve (1991), diameter of the Kara structure as in Nazarov et al. (1993)].**

Crater	Diameter in km	Projectile
Haviland	0.011	pallasite
Dalgaranga	0.021	mesosiderite
Sikhote Alin	0.027	IIAB iron
Campo del Cielo	0.050	IAB iron
Sobolev	0.053	iron
Veevers	0.080	IIAB iron
Wabar	0.097	IIIAB iron
Morasko	0.100	IAB iron
Kaalijärvi	0.110	IAB iron
Henbury	0.157	IIIAB iron
Odessa	0.168	IAB iron
Boxhole	0.170	IIIAB iron
Macha	0.300	iron
Aouelloul	0.390	iron or pallasite
Monturaqui	0.460	IAB iron
Wolfe Creek	0.870	IIIAB iron
Barringer	1.120	IAB iron
<hr/>		
New Quebec	3.400	chondrite
Brent	3.800	L or LL chondrite
Gow	4.000	iron (?)
Ilyinets	4.500	iron
Sääksjärvi	5.000	chondrite
Wanapitei	7.500	LL chondrite
Mien	9.000	stone (?)
Bosumtwi	10.500	iron
Ternovka	12.000	chondrite
Nicholson Lake	12.500	nakhilite or ureilite (?)
Zhamanshin	13.500	chondrite (?)
Dellen	15.000	stone (?)
Obolon	15.000	iron
Lappajärvi	17.000	chondrite
Eñgygytkyn	18.000	achondrite
Clearwater East	22.000	C1 chondrite
Rochechouart	23.000	iron (?)
Ries	24.000	aubrite
Boltysh	25.000	chondrite
Kamensk	25.000	chondrite
Mistastin	28.000	iron (?)
Popigai	100.000	chondrite
Kara	120.000	chondrite

latter one is more effective gaining maximum peak pressure of up to 1000 GPa. These techniques usually use a metal container and plates, and chemical explosives. In the past, gun devices (light-gas or explosive driven) were also applied to provide planar shock waves; maximum dynamic compression achievable by this set up was 30 GPa (Stöffler 1972). The intensity of shock compression is generally given by the character and amount of explosives used in the experiment and dimensions of impacting plates, sample, and the container as well. Although the geometry of the shock wave generated does not correspond to that of a natural impact process, relatively complete information about pressure and temperature during the experiment can be obtained when planar shock wave generators are employed. For detailed discussion of shock recovery experiment of this type see article by Stöffler and Langenhorst (1994).

Non-planar shock waves are much closer to natural conditions and the pressures achieved are higher, however, experiments allowing to model non-planar wave geometry do not provide sufficient information about pressure-temperature conditions of shock wave transitions if any. Stöffler (1972) describes such a device consisting of two or more concentric cylindrical metallic tubes. The inner one is filled with sample and outer one is surrounded by an explosive. After detonation, the outer tube implodes and transmits the convergent shock wave into the sample.

### **Terrestrial impact cratering and environmental crises**

When a large celestial body collides with the Earth, a huge amount of heat is released, converted from the original kinetic energy of the projectile, and the gigantic volume of impact ejecta consisting of fragments of micro- to millimeter dimensions is ejected into the atmosphere.

Experts in many geo-scientific branches over the world have focused their attention on the boundary Cretaceous/Tertiary (K/T) over the last roughly 15 years. At the stratigraphic boundary just mentioned, the last major extinction of the biota occurred. Several estimates indicate that about 80% organisms disappeared during this time (even the lowest estimates give more than 50%). The K/T-boundary is associated with a huge marine biomass loss of planktonic foraminifera, brachiopods, ammonites, bryozoans, many bivalves and gastropods, and calcareous nanoplankton as well. On land, the last of dinosaurs vanished and flowering plants were changed to a short dominance of ferns. Many plant taxa survived, however, to reappear later (McLaren and Goodfellow 1990). Careful study of the boundary over the world has provided several places where the complete stratigraphic sequence is preserved across the boundary studied (e.g. Gubbio in Italy, Stevns Klint in Denmark, Caravaca, Zumaya, Sopolano, Barranco, and Agost in Spain, Woodside Creek, Chancet Rocks and Flaxbourne River in New Zealand, Sumbar in Turkmenia, Raton Basin in Colorado and New Mexico, Hell Creek in Montana (USA), El Kef in Tunisia, Ellendgraben in Austria, several drillcores of the DSDP). Alvarez et al. (1980), after the discovery of Ir and other typically extraterrestrial siderophile group elements and enrichments in boundary strata at Gubbio in Italy, postulated the hypothesis explaining the dinosaurs extinction due to the collision of the Earth with an asteroid Apollo 10 km in diameter. Discovery of a relatively constant content of soot particles in the K/T horizon at Caravaca, Woodside Creek and Stevns Klint showed the possibility of extensive wildfires followed by global cooling and darkness. The K/T catastrophe scenario resembles the "nuclear winter" one, i.e. phenomena possibly occurring after a global nuclear war, though e.g. Wolfbach et al. (1985) pointed out that nuclear winter scenarios were too optimistic compared with events associated with the Cretaceous/Tertiary giant impact. Consequences caused by the K/T Earth-asteroid collision suggested by Wolfbach and others (1990) include: tsunami waves and winds (up to 500 km/h) lasting hours, darkness lasting months, cold, fires, an H<sub>2</sub>O greenhouse effect, the living environment affecting pyrotoxins, acid rain lasting years, a CO<sub>2</sub> greenhouse effect lasting decades, conditions caused by the destruction of the ozone layer, and finally, millennia of the consequences of impact-triggered volcanism and mutagenesis. Finds of minerals with PDFs in deep sea sediments (chiefly quartz and zircon - e.g. Bohor et al. 1984), dating of shocked zircons from the Chicxulub and ejecta deposits in the Raton Basin (Colorado) and Haiti (Krogh et al. 1993), and finds of glassy objects in Haiti (Haiti glasses or K/T-tektites - Izett and others 1990), and later in Mexico, and USA [for further references and glass chemistry see Skála (1993)] in boundary strata have supported the ability of the impact scenario to explain events at the Cretaceous/Tertiary boundary.

When the Chicxulub structure on the Yucatán Peninsula in Mexico, whose diameter is estimated to be 204 km (Sharpton et al. 1993) was found, its impact origin recognized based on geophysical research, and first materials from the crater dated, many scientists started to establish the K/T cataclysm scenario connected to this site. Brett (1992) postulated a new possible lethal mechanism occurring at the K/T boundary since among target materials at the site there are several horizons consisting of evaporites (gypsum and anhydrite) and thus it is very likely that these minerals were thermally decomposed due to shock-compression followed by the post-shock temperature increase. Assuming thermal decomposition of the minerals mentioned, the most probable product of such a reaction is gaseous SO<sub>2</sub> oxidized to SO<sub>3</sub> by later processes in the atmosphere followed by the origin of H<sub>2</sub>SO<sub>4</sub>. Brett's (1992) interesting calculations estimated a crater diameter of 180 km, average target rock density of 2.4, and anhydrite horizon thickness of 500 m at a depth of 1000 m. This resulted in the unbelievable volume of 300 km<sup>3</sup> which was presumably heated to above 1800 K resulting in the release of  $4 \times 10^{17}$  g SO<sub>2</sub>. Such an amount of gaseous SO<sub>2</sub> would mean the formation of some 600 billion tonnes of H<sub>2</sub>SO<sub>4</sub> in the stratosphere which would correspond to 1.2 kg H<sub>2</sub>SO<sub>4</sub> per square meter of the Earth. Eventually, Brett (1992) summarized the possible effects that caused the extinction of terminal Cretaceous biota. These are: (1) stopping photosynthesis by sunshine blocking dust clouds or acidic aerosols (sulfuric or nitric), (2) an initial short heating from the impact instantly followed by cooling by dust particles in the stratosphere, (3) formation of NO<sub>x</sub> contributing to the destruction of a portion of the ozone layer and thus leading to increased UV-radiation, (4) greenhouse effects due to widespread wildfires producing pyrotoxins, mutagens, and soot, finally also reducing photosynthesis, (5) a greenhouse effect caused by vapor injection into the atmosphere, although vapor probably almost instantly crystallized to form ice in the atmosphere and fell out early, (6) a greenhouse effect due to CO<sub>2</sub> injection into the stratosphere (carbon dioxide was released from carbonates during the impact event) resulting in warming up after short initial period of cold caused by the aforementioned effects, and (7) SO<sub>2</sub> release from the shocked sulfate lithologies producing H<sub>2</sub>SO<sub>4</sub>. Gilmour and others (1990) focused their attention on the duration of the K/T-extinction and its selectivity. In addition to enrichment in Ir and other siderophile group elements the boundary horizon is also enriched by As, Sb, and Zn. Based on the oceanic residence times of these elements in sea water which are roughly 10<sup>5</sup> years, the duration of the K/T event can be inferred. Thus, these times do not support alternative hypotheses explaining the extinction by the Deccan volcanic activity, whose time scale is significantly longer - about 0.5 Ma (Gilmour et al. 1990). Moreover, Deccan basalts did not originate precisely at the K/T boundary as indicated by Ar-Ar dating. Selectivity of extinctions associated with the K/T boundary is explained by Gilmour and others (1990) by subsequent events after the collision - chiefly by fallout and acid rain - which severely devastated the marine surface-water living environment. Therefore, the most affected species seem to be calcareous shelled organisms, nektonic marine organisms, and neritic marine organisms (generally considered to be important indicators of marine environment, very sensitive to any environment changes, even in modern times). Similarly, the land flowering plants survived the K/T cataclysm only due to the long dormancy times of their seeds. Occurrence of major wildfires at the K/T boundary is also supported by recent finds of C<sub>60</sub> fullerenes in New Zealand sites (Heymann et al., 1994). According to Deutsch and Schärer (1994), Ar isotopic composition measurements for glassy spherules found at the boundary horizon in Mexico and Haiti have shown that among four candidate crater sites, long thought to possibly be responsible for the K/T event (Manson, Kara, Popigai, Chicxulub), the most likely is Chicxulub in Mexico. This idea is also strongly supported by U-Pb dating of zircon single crystals from the Raton Basin in Colorado, the Beloc site in Haiti, and from the Y6 drill hole within the Chicxulub structure (Krogh et al. 1993) which shows the same age of the precursor for all localities.

Aside from the K/T boundary there are several other boundaries in the Earth history connected with major fauna and/or flora extinctions. These changes of biota can be found at the following boundaries: Precambrian /Cambrian, Ashgill/Llandovery (Late Ordovician), Frasnian/Famennian (Devonian), Devonian/Carboniferous, Permian/Triassic, and Eocene/Oligocene. McLaren and Goodfellow (1990) discussed these stratigraphic boundaries in detail with respect to the geochemical and sedimentological signature of each boundary, character of biomass loss, and also the possibility of extraterrestrial causes of the extinction.

The Cenozoic boundary Eocene/Oligocene whose radiometric age is 34.5 Ma does not represent global extinctions of such scale as those recorded at the K/T boundary. Nevertheless, a major evolutionary break occurs at this horizon (McLaren and Goodfellow 1990). This break is characterized by changes in planktonic foraminifera, gastropods, bivalves and mammalian fauna in North America and Asia (or replacement at an accelerated rate). Similarly, abrupt changes occurred in amphibia and reptiles in Europe at the same time. Near the horizon boundary, there are two iridium anomalies in the sedimentary record and finds of American tektites and microtektites (these are known from Barbados and the whole marine area of central America).

The terminal Triassic biota characterized by its highly diverse fauna was at the Triassic/Jurassic boundary replaced initially and briefly by a very reduced one and only later on replaced by molluscan and ammonite faunas typical of Jurassic. Enrichment of the boundary layer in Ir, Fe, P, Y, La, Yb, Zn, As, and Sb is, as stressed by McLaren and Goodfellow (1990), rather of terrestrial origin. None of known terrestrial impact craters corresponds by its absolute age to that of the boundary mentioned.

The most global Phanerozoic extinctions occurred at the Upper Permian and included both marine organisms and land vertebrates and plants. This biota reduction affected about 90 to 96% marine invertebrate species, all but one of 90 genera of reptiles, and complete *Glossopteris* flora of Gondwana (McLaren and Goodfellow 1990 and references therein). Geochemical sections through the horizon containing the boundary reveal changes in isotopic composition of carbon, strontium, and sulfur. Final global extinction of environmentally stressed Permian biota is thus very probably related to the impact of an extraterrestrial body which represents an unusual energetic event.

The Devonian/Carboniferous boundary is characterized according to McLaren and Goodfellow (1990) by disappearing of diverse and abundant ammonoid faunas of the highest Famennian (genus *Wolchumeria*) from which only one or two genera survived, followed by spreading of the earliest Carboniferous ammonites (genera *Gattendorfia* and *Imitoceras*). Aside from ammonites a similar trend of the diversity and biomass reduction was observed for trilobites and conodonts. Geochemical anomalies with increased content of Ir, Pt, Os, and Au present across the boundary in form of four individual horizons, however, do not correspond to the signature of an impact of an extraterrestrial body. Nevertheless, the possibility remains that siderophile group elements enrichments are of meteoritic origin but have been extensively reworked by sedimentary processes and differential mobilization of PGE (McLaren and Goodfellow 1990 and references therein).

Based on observations of the major biotic change on four continents the biostratigraphic boundary Frasnian/Famennian (F/F) was set as a horizon where massive biomass reduction occurred. Extinctions were sudden and probably synchronous worldwide as it is apparent from the fossil record in basins, shelf margins, midshelf and shallow water environments. Geochemical section across the F/F boundary reveals significant enrichment in Ir and other siderophile elements very similar to that of K/T. McLaren and Goodfellow (1990) therefore suggested as a probable cause of the F/F event an impact of an extraterrestrial body about 367 Ma ago. Recent finds of spherical glassy objects resembling microtektites from Dinant basin in Belgium (localities Hony and Senzeille) and from Quindong in China (Clayes and Cassier 1993) strongly support this idea in the same way as the Haiti glasses did for the K/T boundary. According to Clayes and Cassier (1993), possible candidates for F/F impact crater site are structures Charlevoix in Canada, whose diameter is 52 km and K-Ar age 350(20) Ma, and Siljan in Sweden with diameter of 52 km and  $^{40}\text{Ar} - ^{39}\text{Ar}$  age of 368(1) Ma. Target materials are chemically closer to the above mentioned "microtektites" in Siljan than that encountered in the crater Charlevoix.

Close to the base of Silurian, which is defined at a stratotype at Moffat in Scotland as a base of a graptolite biozone *Akidograptus acuminatus*, there were found layers characterized by sudden biomass loss and enrichment in siderophile elements in Ordovician strata corresponding to Ashgillian in many places over the world (Britain, Scandinavia, China, America). Aside from other hypotheses explaining Late Ordovician extinction involving such reasons as climatic deterioration and glacial-eustatic draining of epicontinental seas, several authors assumed that an impact might have influenced this extinction. Sedimentologic studies of the Ashgillian/Llandovery sections provide information about events preceding the biomass reduction; glacial period and ocean regression was followed by a major worldwide transgression. This sequence can also be explained by the impact of a huge meteorite or a comet crashing into the ocean. The probable consequences of such an impact resemble those known from the K/T boundary (McLaren and Goodfellow 1990 and references therein).

The first boundary in the Earth's history when major biotic change occurred is that of the Precambrian/Cambrian. However, a definition of this boundary is still under discussion due to difficulties in correlating intercontinentally all the necessary information (particularly geochemical data, chiefly PGE contents and carbon isotopic changes). Early metazoan-like fossils are known from rocks dated as old as 650-610 Ma. They are assigned to the Vendian Series and earlier (Riphean). Small shelled fossils first appeared in the Tommotian. First trilobites were found in rocks of the Atdabanian age. Protometazoan faunas referred to as the Ediacaran seem to overlap in range with small shelled fossils. Therefore, the question is where the boundary should be set. It can be assigned to the base of either the Atdabanian or Tommotian. A large reduction in biomass was reported from the Tommotian/Atdabanian boundary. This boundary in China (Precambrian C) is also associated with an abrupt change in the character of the sedimentary record (from phosphatic-rich rocks to black shales), a negative shift of  $\delta^{13}\text{C}$  values and PGE anomalies. However, the age of the Lake Acraman impact structure in South Australia - one of the biggest impact crater in the world - is older than that of the Tommotian/Atdabanian extinction mentioned (McLaren and Goodfellow 1990).

## Impacts and civilization

Up to 1994, when the article of Yau and others (1994) appeared, no human fatalities had been reported in connection with collisions of extraterrestrial materials with the Earth. However, a dog was killed when meteorite Nakhla fell in Egypt, meteorites have pierced the roofs of houses on several occasions, and on October 9, 1992, a meteorite in the American city Peekskill penetrated the roof of a parked car (fortunately empty at the time of collision since the passengers were visiting a football match at a nearby stadium) and damaged it significantly. Yau et al. (1994) found, in historical Chinese texts, evidence that meteorites killed many human beings in historic China. More than 10 people were killed by a meteorite or bolide explosion on January 14, 616. In 14th century several meteorites or meteoritic showers fell (mainly irons) and struck people and some of them died. More than 10000 people were killed in 1490 when a shower of stony meteorites (larger stones of 1.5 kg, smaller ones of 1 kg mass) fell in the Ch'ing-yang district. Several human beings were killed by a large stony meteorite that fell on a small market street in 1639. A child was killed by a stone that fell suddenly at Chin-kuei Shan in Ming-tung Li. All of Wang Teng-kuei's family died when a stone fell at Hsin-p'ai Wei in Weng-li on September 5, 1907.

The answer to the question whether modern civilization is jeopardized by a possible collision of the Earth with an asteroid or a comet of large dimensions is given in a recent paper by Chapman and Morrison (1994). In addition to the Sun, planets, and their moons, the Solar system consists of many other bodies with dimensions ranging from fractions of a micrometer to tens or hundreds of meters in diameter. This interplanetary matter, in the form of interplanetary dust, comets, meteoroids, and asteroids moves through the Solar system on numerous trajectories of which many are still not well defined. Trajectories of many cosmic bodies lying in the main asteroid belt between Mars and Jupiter are heavily influenced by the gravity fields of large jovian planets. Therefore, some of the celestial bodies cross the trajectory of the Earth and it becomes the target of cosmic collisions of various scales. Civilization of the Earth itself can be endangered by the collision with an asteroid some hundreds meters in diameter or even larger. Asteroids capable of causing a global catastrophe on the Earth exist and are called ECA (Earth Crossing Asteroids) or NEA (Near Earth Asteroids). The flux of these bodies in the vicinity of the Earth can be inferred from the undisturbed impact record on the Moon plains younger than 3.0 Ga. By the end of 1992, a total of 163 ECAs were catalogued; the biggest one is called 1627 Ivar and its diameter reaches 8 km. However, the completeness of such a list of ECAs significantly decreases as the diameter of these asteroids decreases, thus the degree of completeness for bodies, whose diameter is larger than 1 km, is about 5%, and for objects 100 meters across the degree is estimated to be 0.1% only. The comet flux is much lower than the asteroid one, however, comets travel through space by velocities larger than those of asteroids (asteroids travel typically at 20 km/sec speed and the typical velocity for short-period comets ranges between 30-40 km/sec and for long-period ones even varies between 50-60 km/sec), so comets have considerably higher kinetic energies than similarly sized asteroids and therefore constitute a significant share (about 25%) of the impact hazard.

Chapman and Morrison (1994) divided possible hazards induced by the collision of the Earth with larger fragments of the extraterrestrial matter into three groups according to probable consequences of an impact. Though Yau et al. (1994) reported some human casualties caused by meteorite falls from medieval China, common meteorite falls do not represent serious risk for humankind. Since the Earth atmosphere is a significant barrier to cosmic impactors, even at megaton energies, most meteoroids break up and are consumed before they reach the lower atmosphere; these bodies which do not collide with the Earth surface are called fireballs or, when they explode, bolides. To penetrate the lower atmosphere and reach the terrestrial surface, a non-iron projectile has to have energy of 10 MT (1 MT =  $4.2 \times 10^{15}$  J; just for comparison, the Hiroshima nuclear bomb energy was 0.015 MT) or 50 meters across at 20 km/sec speed. Concerning frequency of these phenomena, a few events of such a scale are expected each century. Locally devastating impacts are according to Chapman and Morrison (1994) those produced by stony or metallic projectiles 250 m across or larger, inducing the formation of craters 5 km in diameter or larger when striking the Earth. A certain type of impact of smaller scale, serving as a good calibration for larger events, is represented by the 1908 Tunguska airburst, when due to the in air explosion of a cometary nucleus trees were fallen over an area of 1000 km<sup>2</sup> and the succeeding fireball ignited fires over smaller areas. The energy released during the Tunguska event has been estimated to be 10 to 20 MT. The probability of 1000 MT event was estimated to happen every 10000 years, what means, expressed as percentage during one lifetime, 1% probability. The corresponding area of devastation reaches 10<sup>4</sup> km<sup>2</sup> or 0.002% of the Earth's surface. Generally, the lethal area due to similarly scaled impacts is given by  $A = 100 Y^{2/3}$ , where Y is yield in MT and A represents the area in km<sup>2</sup>. The globally catastrophic impacts are, according to Chapman and Morrison (1994), those disrupting global agricultural production and leading both directly and indirectly to the death of more than a quarter of world population (i.e. about more than 1.5 billion people). Global catastrophe just defined can be caused by the impact of an extraterrestrial body 1 to 2 km across striking the Earth at 20 km/sec. The energy released during such an impact reaches 10<sup>5</sup> to 10<sup>6</sup> MT sufficient to eject 10<sup>16</sup> g of dust particles into the stratosphere - an amount 100-times higher than that ejected into the stratosphere by volcanic eruptions during the last two centuries. Dust particles would then cause the blocking of light resulting in a depressing of the average land temperature by 10 °C or more for a period of months to as long as a year. The statistical probability of a collision of such a scale is one per  $5 \times 10^5$  years. Fatality rates, impactor dimensions and energy yields for selected impact events are summarized in Table 7. From the point of view of frequency and death probability (see Fig. 22) the impacts represent extreme cases of rare but high consequence hazards. Table 8 lists several type of hazards as exemplified by USA population and compares them with those caused by global impact induced cataclysm. Chapman and Morrison (1994) finally concluded, that the chances that civilization might be disrupted or even destroyed by a major impact are very low, but they are not zero.

**Table 7. Fatality rates, projectile diameter and energy release for selected impact events (from Chapman and Morrison, 1994).**

Type of event	Diameter of impactor	Energy in MT	Typical interval in yr.	Estimated deaths	World deaths per year
High atmospheric break-up	< 50 m	< 9	n.a.	0	0
Tunguska-like events	20-300 m	9 - 2 000	250	$5 \times 10^3$	20
Large sub-global events	300 - 600 m	$2\ 000 - 1.5 \times 10^4$	$35 \times 10^3$	$3 \times 10^5$	8
	300 - 1 500 m	$2\ 000 - 2.5 \times 10^5$	$25 \times 10^3$	$5 \times 10^5$	20
	300 - 5 000 m	$2\ 000 - 10^7$	$25 \times 10^3$	$1.2 \times 10^6$	45
<b>Low global threshold</b>	<b>&gt; 600 m</b>	<b><math>1.5 \times 10^4</math></b>	<b><math>7 \times 10^4</math></b>	<b><math>1.5 \times 10^9</math></b>	<b><math>2 \times 10^4</math></b>
<b>Nominal global threshold</b>	<b>&gt; 1.5 km</b>	<b><math>2 \times 10^5</math></b>	<b><math>5 \times 10^5</math></b>	<b><math>1.5 \times 10^9</math></b>	<b><math>3 \times 10^3</math></b>
<b>High global threshold</b>	<b>&gt; 5 km</b>	<b><math>1 \times 10^7</math></b>	<b><math>6 \times 10^6</math></b>	<b><math>1.5 \times 10^9</math></b>	<b>250</b>
Rare K/T scale events	> 10 km	$1 \times 10^8$	$1 \times 10^8$	$5 \times 10^9$	50

**Table 8. Chances of dying due to selected causes in the USA (from Chapman and Morrison, 1994)**

Cause of death	Chances
Motor vehicle accident	1 in 100
Murder	1 in 300
Fire	1 in 800
Firearms accident	1 in 2 500
<b>Asteroid/comet impact (lower limit)</b>	<b>1 in 3 000</b>
Electrocution	1 in 5 000
<b>ASTEROID/COMET IMPACT</b>	<b>1 in 20 000</b>
Passenger aircraft crash	1 in 20 000
Flood	1 in 30 000
Tornado	1 in 60 000
Venomous bite or sting	1 in 100 000
<b>Asteroid/comet impact (upper limit)</b>	<b>1 in 250 000</b>
Fireworks accident	1 in 1 million
Food poisoning by botulism	1 in 3 million
Drinking of EPA limit of TCE	1 in 10 million

EPA, Environmental Protecting Agency; TCE, trichloroethylene.

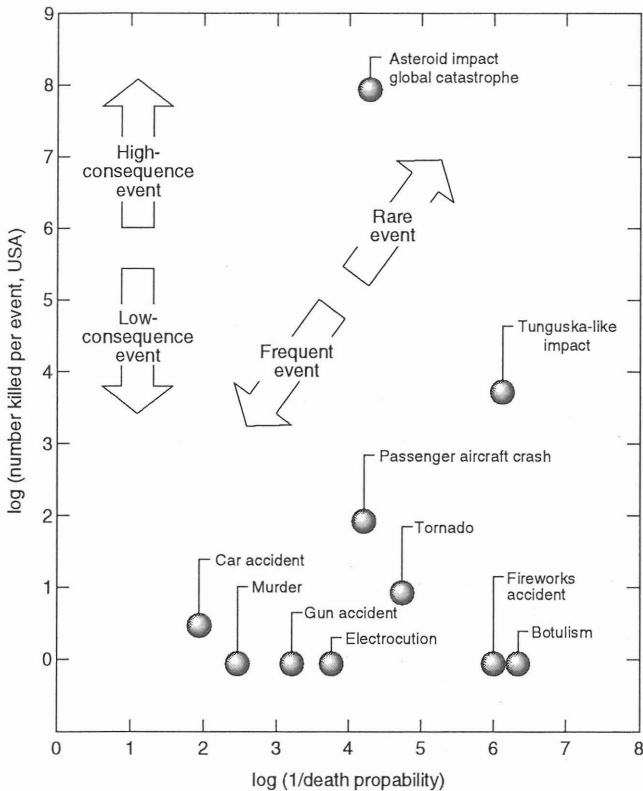


**Fig. 22. Graph of two impact events indicating inverse death probability vs. number of killed in the event. High-consequence and low-consequence as well as rare and frequent event trends are indicated by arrows. (After Chapman and Morrison 1994).**

## Acknowledgments

This review article is based on the author's study of the impact process which is partially covered by the Grant Agency of the Czech Republic (project No. 205/95/0980). The author is also very indebted to Dr. Ann Theriault of the Geological Survey of Canada for providing the most current list of impact structures including target materials, and to Drs. Petr Jakeš and Martin Šolc of Charles University, and Dr. Marcela Bukovanská of the National Museum in Prague, for their helpful discussions on various aspects of the problem.

## References

- Alvarez L. W., Alvarez W., Asaro F., Michel H. V. (1980): Extraterrestrial cause for the Cretaceous-Tertiary extinction. - *Science*, 208: 1095-1108.
- Austrheim H., Boundy T. M. (1994): Pseudotachylites generated during seismic faulting and eclogitization of the deep crust. - *Science*, 265: 82-83.
- Bohor B. F., Foord E. E., Modreski P. J., Triplehorn D. M. (1984): Mineralogic evidence for an impact event at the Cretaceous-Tertiary boundary. - *Science*, 224: 867-869.
- Bouška V., Borovec Z., Cimbáliková A., Kraus I., Lajčáková A., Pačesová M. (1987): Přírodní skla. [Natural glasses]. - *Academia, Praha*, 264 pp. (in Czech).
- Bouška V., Vrána S. (1993a): Impaktový proces. [Impact process]. - *Geol. Průzk.*, 35: 211-215. (in Czech).
- Bouška V., Vrána S. (1993b): Energetická bilance impaktového a ostatních geologických procesů [Energy balance of impact and other geological processes]. - *Geol. Průzk.*, 35: 274-278 (in Czech).
- Chan C.-I., Wu S., Luo X. (1992): Hong Kong is an impact crater: Proof from the geomorphological and geological evidence. - *Int. Conf. On Large Meteorite Impacts and Planetary Evolution, Sudbury*, p. 12.
- Chao E.T.C., Shoemaker E.M., Madsen B.M. (1960): First natural occurrence of coesite. - *Science*, 132: 220-222.
- Chao E. T. C., Fahey J. J., Littler J., Milton D. J. (1962): Stishovite, SiO<sub>2</sub>, a very high pressure new mineral from Meteor Crater, Arizona. - *J. Geophys. Res.*, 72: 419-421.
- Chao E. T. C., Hüttner R., Schmidt-Kaler H. (1978): Principal Exposures of the Ries Meteorite Crater in Southern Germany. Description, photographic documentation and interpretation. - *Bayerisches Geologisches Landesamt, München*, 84 pp.
- Chapman C. R., Morrison D. (1994): Impact on the Earth by asteroids and comets: assessing the hazard. - *Nature*, 367: 33-40.
- Chopin C. (1984): Coesite and pure pyrope in high-grade blueschists of the Western Alps: A first record and some consequences. - *Contrib. Min. Petrol.*, 86: 107-118.
- Clayes P., Casier J.-G. (1993): Microtektite-like glass spherules in late Devonian (367 Ma) shales. - *Lun. Planet. Sci. Conf.*, XXIV: 295-296.
- Cordier P., Vrána S., Doukhan J.C. (1994): Shock metamorphism in quartz at Sevetin and Susice (Bohemia)? A TEM investigation. - *Meteoritics*, 29: 98-99.
- Deutsch A., Schärer U. (1994): Dating terrestrial impact events. - *Meteoritics*, 29: 301-322.
- Engelhardt W. von, Bertsch W. (1969): Shock induced planar deformation structures in quartz from the Ries crater, Germany. - *Contr. Mineral. Petrol.*, 20: 203-234.
- French B. M. (1990): 25 years of the impact-volcanic controversy. Is there anything new under the Sun or inside the Earth? - *EOS*, 71: 411-414.
- Gilmour I., Wolfbach W.S., Anders E. (1990): Early environmental effects of the terminal Cretaceous impact. - In: Sharpton V. L. and Ward P. D. (eds.): *Global catastrophes in Earth history*, Geol. Soc. Amer., Spec. Pap., 247: 383-390.
- Gostin V. A., Keays R. R., Wallace M. W. (1992): The Acraman impact and its widespread ejecta, South Australia. - *Int. Conf. On Large Meteorite Impacts and Planetary Evolution, Sudbury*, 30-31 pp.
- Grieve R.A.F. (1987): Terrestrial impact structures. - *Ann. Rev. Earth Planet. Sci.*, 15: 245-270.
- Grieve R. A. F. (1990): Impact cratering on the Earth. - *Scientific American*, April 1990, 66-73 pp.
- Grieve R. A. F. (1991): Terrestrial impact: The record in the rocks. - *Meteoritics*, 26: 175-194.
- Grieve R. A. F. (1993): written communication - list of impact structures.
- Grieve R. A. F., Cintala M. J. (1992): An analysis of differential impact melt-crater scaling and implications for the terrestrial impact record. - *Meteoritics*, 27, 526-538.
- Hemley R. J., Prewitt C. T., Kingma K. J. (1994): High-Pressure Behavior of Silica. - In: P. J. Heaney, C. T. Prewitt and G. V. Gibbs (eds.): *Silica, Reviews in Mineralogy*, Vol. 29: 41-81.
- Heymann D., Chibante L. P. F., Brooks R. R., Wolfbach W. S., Smalley R. E. (1994): Fullerenes in the Cretaceous-Tertiary boundary layer. - *Science*, 265: 645-647.
- Izett G. A., Maurrasse F. J.-M. R., Lichte F. E., Meeker G. P., Bates R. (1990): Tektites in Cretaceous-Tertiary boundary rocks on Haiti. - *USGS Open File Report 90-635*, 31 pp.

- Kieffer S. W., Phakey P. P., Christie J. M. (1976): Shock processes in porous quartzite: Transmission electron microscope observations and theory. - *Contr. Mineral. Petrol.*, 59: 41 - 93.
- Kikuchi M., Syono Y., Velde B. (1993): Shock wave effects on kaolinite and other clays. - *Amer. Mineral.*, 78: 904-940.
- Koeberl C., Reimold W. U., Powell R. A. (1994): Shocked quartz and impact melt rock at the Ames structure, Oklahoma. - *Abstract, Meteoritics*, 29: 483.
- Kopecný (1993): Význam armalcolitu v suevitovém tufu pro řešení vzniku matečného kráteru vltavínů. [Significance of armalcolite in suevitic tuff for solving of an origin of parent moldavite crater]. - *Geol. Průzk.*, 35: 219-222. (in Czech).
- Krogh T.E., Kamo S.E., Sharpton V.L., Marin L.E., Hildebrand A.R. (1993): U-Pb ages of single shocked zircons linking distal K/T ejecta to the Chicxulub crater. - *Nature*, 366: 731-734.
- Marvin U. B. (1990): Impact and its revolutionary implications for geology. - In: Sharpton V.L. and Ward P.D. (eds.): *Global catastrophes in Earth history*, *Geol. Soc. Amer., Spec. Pap.*, 247: 147-154.
- Marvin U. B. (1992): The meteorite of Ensisheim. - *Meteoritics*, 27: 28-72.
- Marvin U. B. (1994): Ernst F.F. Chladni (1756-1827) and the beginnings of meteoritics. - *Abstract, Meteoritics*, 29: 496-497.
- Masaitis V. L. (1992): Impact craters: Are they useful? - *Meteoritics*, 27: 21-27.
- Masaitis V. L. (1992): Impactites from Popigai crater. - *Int. Conf. On Large Meteorite Impacts and Planetary Evolution, Sudbury*, p. 51.
- Masaitis V. L., Danilin A. N., Mašák M. S., Rajchlin A. I., Selikanovskaja T. V., Šadenkov E. M. (1980): *Geologia astroblesm [Geology of astroblemes]*. - Nedra, Leningrad, 231 pp. (in Russian).
- McLaren D. J., Goodfellow W. D. (1990): Geological and biological consequences of giant impacts. - *Ann. Rev. Earth Planet. Sci.*, 18: 123-171.
- Melosh H. J. (1989): *Impact Cratering. A Geologic Process*. - Oxford University Press, 245 pp.
- Mittlefehldt D. W., Snee T. H., Hörz F. (1992): Dissemination and fractionation of projectile materials in the impact melts from Wabar Crater, Saudi Arabia. - *Meteoritics*, 27: 361-370.
- Müller-Mohr V. (1992): Sudbury project (University of Münster - Ontario Geological Survey): (5) New investigations on Sudbury breccia. - *Int. Conf. On Large Meteorite Impacts and Planetary Evolution, Sudbury*, p. 53.
- Nazarov M. A., Badjukov D. D., Alekseev A. S., Kolesnikov E. M., Kaškarov L. L., Barsukova L. D., Suponeva I. V., Kolesov G. M. (1993): Karskaja udarnaja struktura i jejo svjaz s mel-paleogenoveym sobytiem [Kara impact structure and its connection to Cretaceous/Paleogene event]. - *Bjul. Mosk. O-va. Ispytatelej prirody*, otd. geol., 68(3): 13-32. (in Russian).
- Nininger H. H. (1956): *Arizona's Meteorite Crater. Past - Present - Future*. - American Meteorite Museum, Sedona, Arizona, 232 pp.
- Okay A. I., Shutong X., Sengor A. M. C. (1989): Coesite from Dabie Shan eclogites, central China. - *Eur. J. Mineral.*, 1: 595-598.
- Papagiannis M. D. (1989): Photographs from geostationary satellites indicate the possible existence of a huge 300 km impact crater in the Bohemian region of Czechoslovakia. - *Abstracts for the 52nd Annual Meeting of the Meteoritical Society, Vienna*, p. 189.
- Rajlich P. (1992): Bohemian circular structure, Czechoslovakia: Search for the impact evidence. - *Int. Conf. On Large Meteorite Impacts and Planetary Evolution, Sudbury*, 57-59 pp.
- Reimold W. U., Collinson W. P. (1992): The pseudotachylites from the Vredefort structure and the Witwatersrand basin. - *Int. Conf. On Large Meteorite Impacts and Planetary Evolution, Sudbury*, 60-61 pp.
- Rondot J. (1989): Pseudotachylite and mylonitization. - *Abstracts for the 52nd Annual Meeting of the Meteoritical Society, Vienna*, p. 209.
- Schmidt R. M., Housen K. R. (1987): Some recent advances in the scaling of impact and explosion cratering. - *Inter. J. Impact Eng.*, 5: 543-560.
- Sharpton V. L., Burke K., Hall S. A., Lee S., Marín L. E., Suarez G., Quezada-Mu eton J. M., Urrutia-Fucugauchi J. (1993): Chicxulub impact basin: Gravity characteristics and implications for basin morphology and deep structure. - *Lun. Planet. Sci. Conf.*, XXIV: 1283-1284.
- Skála R. (1993): Haitská skla - pravděpodobně nejstarší známé tektity. [Haiti glasses - probably the oldest known tektites.] - *Geol. Průzk.*, 35: 285-289. (in Czech)
- Skála R. (1994): *Impaktové kráterování Země [Impact cratering of the Earth]*. - *Bull. min.-petr. odd. NM v Praze*, 2: 38-62. (in Czech).
- Smyth J. V., Hatton C. J. (1977): A coesite-sanidine grosspydite from the Roberts Victor kimberlite. - *Earth Planet. Sci. Lett.* 34: 284-290.
- Sobolev N. V., Yefimova E. S., Koptil V. I., Lavrentyev Y. G., Sobolev V. S. (1976): Inclusions of coesite, garnet, and omphacite in Yakutian diamond: First discovery of coesite paragenesis. - *Dokl. Akad. Nauk SSSR*, 230: 1441-1444.
- Spray J. G. (1993): Delimitation of terrestrial impact craters via pseudotachylitic rock distribution. - *Lun. Planet. Sci. Conf.*, XXIV: 1335-1336.

- Stöffler D. (1971): Progressive metamorphism and classification of shocked and brecciated crystalline rocks at impact craters. - *J. Geophys. Res.*, 76: 5541 - 5551.
- Stöffler D. (1984): Glasses formed by hypervelocity impact. - *J. Non-Crystalline Solids*, 67: 465-502.
- Stöffler D. (1972): Deformation and transformation of rock-forming minerals by natural and experimental shock processes. I. Behavior of minerals under shock compression. - *Fortschr. Miner.*, 49: 50-113.
- Stöffler D. (1974): Deformation and transformation of rock-forming minerals by natural and experimental shock processes. II. Physical properties of shocked minerals. - *Fortschr. Miner.*, 51: 256-289.
- Stöffler D., Langenhorst F. (1994): Shock metamorphism of quartz in nature and experiment: I. Basic observation and theory. - *Meteoritics*, 29: 155-181.
- Stöffler D., Grieve R. A. F. (1994): Classification and nomenclature of impact metamorphic rocks: A proposal the IUGS Subcommission on the Systematics of Metamorphic Rocks. - (classification of impactites presented during Houston LPS Conference held in March in 1994, unpublished).
- Stöffler D., Keil K., Scott E. R. D. (1991): Shock metamorphism of ordinary chondrites. - *Geochim. Cosmochim. Acta*, 55: 3846-3867.
- Taylor S. R. (1982): *Planetary Science: A Lunar Perspective*. - Lunar and Planetary Institute, Houston, 481 pp.
- Vrána S. (1987): The Ševětín astrobleme, southern Bohemia, Czechoslovakia. - *Geol. Rundschau*, 76: 505-528.
- Vrána S., Bendl J., Buzek F. (1993): Pyroxene microgranodiorite dykes from the Ševětín structure, Czech Republic: mineralogical, chemical, and isotopic indication of a possible impact melt origin. - *J. Czech Geol. Soc.*, 38: 129-146.
- Wang X., Liou J. G., Mao K. H. (1989): Coesite-bearing eclogite from the Dabie Mountains in central China. - *Geology*, 12: 1085-1088.
- White J. C. (1992): Electron petrography of silica polymorphs associated with pseudotachylites, Vredefort structure, South Africa. - *Int. Conf. On Large Meteorite Impacts and Planetary Evolution, Sudbury*, 78-79 pp.
- Wolfbach W. S., Lewis R. S., Anders E. (1985): Cretaceous extinctions: Evidence for wildfires and search for meteoritic material. - *Science*, 230: 167-170.
- Wolfbach W. S., Gilmour I., Anders E. (1990): Major wildfires at the Cretaceous / Tertiary boundary. - In: Sharpton V.L. and Ward P.D., (eds.): *Global catastrophes in Earth history*. - *Geol. Soc. Amer., Spec. Pap.*, 247: 391-399.
- Yau K., Weissman P., Yeomans D. (1994): Meteorite falls in China and some related human casualty events. - *Meteoritics*, 29: 864-871.